

EVOLUTIONARY BIOLOGY

Gene losses in the common vampire bat illuminate molecular adaptations to blood feeding

Moritz Blumer^{1,2,3,4,†}, Tom Brown¹, Mariella Bontempo Freitas⁵, Ana Luiza Destro⁵, Juraci A. Oliveira⁶, Ariadna E. Morales^{4,7,8}, Tilman Schell^{7,8}, Carola Greve^{7,8}, Martin Pippel¹, David Jebb^{1,2,3}, Nikolai Hecker^{1,2,3}, Alexis-Walid Ahmed^{4,7,8}, Bogdan M. Kirilenko^{4,7,8}, Maddy Foote⁹, Axel Janke^{7,10}, Burton K. Lim¹¹, Michael Hiller^{1,2,3,4,7,8,*}

Vampire bats are the only mammals that feed exclusively on blood. To uncover genomic changes associated with this dietary adaptation, we generated a haplotype-resolved genome of the common vampire bat and screened 27 bat species for genes that were specifically lost in the vampire bat lineage. We found previously unknown gene losses that relate to reduced insulin secretion (*FFAR1* and *SLC30A8*), limited glycogen stores (*PPP1R3E*), and a unique gastric physiology (*CTSE*). Other gene losses likely reflect the biased nutrient composition (*ERN2* and *CTRL*) and distinct pathogen diversity of blood (*RNASE7*) and predict the complete lack of cone-based vision in these strictly nocturnal bats (*PDE6H* and *PDE6C*). Notably, *REP15* loss likely helped vampire bats adapt to high dietary iron levels by enhancing iron excretion, and the loss of *CYP39A1* could have contributed to their exceptional cognitive abilities. These findings enhance our understanding of vampire bat biology and the genomic underpinnings of adaptations to blood feeding.

INTRODUCTION

Vampire bats are the only obligate sanguivorous lineage among tetrapods (1). This exceptional dietary specialization is reflected in all aspects of their biology, including morphology, physiology, and behavior (2). To detect prey, the common vampire bat (*Desmodus rotundus*) exhibits a well-developed olfactory system (3), advanced low-frequency hearing abilities (4), and, unique among mammals, the ability to sense infrared radiation (5). Compared to other bats, vampire bats have exceptional terrestrial locomotion skills to sneak up on their prey (6). Razor-sharp enamel-less upper incisors help cut through the prey's skin, and anticoagulants in their saliva prevent the prey's blood from coagulating during feeding (7, 8).

As the sole nutritional source, blood represents a challenging diet for several reasons. First, blood has a high fluid content of 78% and a comparatively low caloric value, making it necessary for a vampire bat to ingest as much as 1.4 times their body weight in blood during a single meal (9). To enable the ingestion of large amounts of blood, their stomach experienced a functional shift toward a distensible organ primarily engaged in storage and fluid absorption. Second, blood has a high iron content compared to other diets, which mainly stems from hemoglobin-derived heme and ferric iron transported by transferrin (10–12). Third, the dry mass

of blood has a highly skewed nutritional composition, providing mostly proteins (93%) with very little lipids and carbohydrates (1% each) (9).

Because of low carbohydrate intake, vampire bats exhibit lower basal insulin levels than other mammals (9, 13). Similar to human type 2 diabetes patients, vampire bats feature a reduced glucose-stimulated insulin secretion response, resulting in hyperglycemia upon an experimental glucose overload (13). Glycogen and lipid stores are also reduced in vampire bats, which contributes to their fasting vulnerability and early deaths after 48 to 72 hours of fasting (14, 15). To compensate for their fasting vulnerability, vampire bats share regurgitated blood with roost mates that failed to obtain a nightly meal (16).

To gain insights into the molecular basis of vampire bat adaptations to sanguivory, comparative studies using the genome of the common vampire bat detected signatures of selection in genes involved in responses to nutrient starvation, metabolism, nitrogen waste disposal, the coagulation cascade, and immunity (17, 18). Common vampire bats have fewer *TAS2R* taste receptor genes than other bats, indicating a reduced sense of bitter taste reception (19, 20). In addition to genetic changes, vampire bats also have a gut microbiome very different from that of other bats, and genes encoded by their gut microbiome further contribute to meeting the challenges of sanguivory (17). Despite these advances, our understanding of which genomic changes are important for adaptations to sanguivory remains incomplete.

A limitation of previous comparative studies was the restricted taxonomic representation. *D. rotundus* belongs to the family of leaf-nosed bats (Phyllostomidae), which comprises more than 220 species (<https://batnames.org>). While Zepeda Mendoza *et al.* (17) compared the *D. rotundus* genome to nine other bat genomes, *D. rotundus* was the only representative of phyllostomid bats in their study. With this limited taxonomic resolution, one cannot differentiate between those genomic changes that are shared between all phyllostomid bats and those changes that evolved specifically in the vampire bat lineage and thus could be relevant for adaptations

¹Max Planck Institute of Molecular Cell Biology and Genetics, 01307 Dresden, Germany.

²Max Planck Institute for the Physics of Complex Systems, 01187 Dresden, Germany.

³Center for Systems Biology Dresden, 01307 Dresden, Germany. ⁴Goethe University, Faculty of Biosciences, Max-von-Laue-Str. 9, 60438 Frankfurt, Germany. ⁵Department of Animal Biology, Federal University of Viçosa, Viçosa, Brazil. ⁶Department of General Biology, Federal University of Viçosa, Viçosa, Brazil. ⁷LOEWE Centre for Translational Biodiversity Genomics, Senckenberganlage 25, 60325 Frankfurt, Germany. ⁸Senckenberg Research Institute, Senckenberganlage 25, 60325 Frankfurt, Germany. ⁹Native Bat Conservation Program, Toronto Zoo, 361A Old Finch Avenue, Toronto, Ontario M1B 5K7, Canada. ¹⁰Senckenberg Biodiversity and Climate Research Centre, Senckenberganlage 25, 60325 Frankfurt am Main, Germany.

¹¹Department of Natural History, Royal Ontario Museum, 100 Queen's Park, Toronto, Ontario M5S 2C6, Canada.

*Corresponding author. Email: michael.hiller@senckenberg.de

†Present address: Department of Genetics, University of Cambridge, Downing Street, Cambridge CB2 3EH, UK.

to sanguivory. To uncover genomic changes that evolved specifically in the vampire bat lineage, we generated a state-of-the-art haplotype-resolved chromosome-level assembly of *D. rotundus* and made use of 26 other currently available bat genomes, including six phyllostomid species. Since the loss of ancestral genes can be an important evolutionary force and previous studies revealed many associations between gene losses and phenotypic differences, including dietary adaptations (21–24), we conducted a genome-wide screen for genes that are specifically lost in *D. rotundus*. This screen revealed 3 known and 10 previously unknown gene losses. Many of these novel gene losses have clear associations with vampire bat traits, and some gene losses may contribute to coping with the challenges imposed by sanguivory.

RESULTS AND DISCUSSION

A new haplotype-resolved reference-quality *D. rotundus* assembly

To perform an accurate and comprehensive screen for gene losses in the common vampire bat, a genome assembly with high completeness, contiguity, and base accuracy is desirable. The existing Illumina assembly of the common vampire bat (17) has more than 50,000 assembly gaps, indicating that a subset of genes will have missing sequences. This assembly also exhibits base errors that mimic gene-inactivating mutations, including cases where multiple putative mutations in the same gene are all erroneous (fig. S1). Therefore, we generated a new reference-quality *D. rotundus* assembly. We used PacBio circular consensus (HiFi) sequencing to produce 32× coverage in reads with an average length of 9.1 kb and used the Dovetail Omni-C protocol to produce 67× coverage of chromosome conformation capture Illumina read pairs. With these data, we obtained two haplotype-resolved chromosome-level assemblies that have only 596 and 557 assembly gaps, contig N50 values of 6.85 and 7.98 Mb, and scaffold N50 values of 160.1 and 160.1 Mb (Fig. 1A and table S1). The contig N50 metric is ~90 times higher than that of the Illumina-based *D. rotundus* assembly (17). The karyotype of *D. rotundus* is $2n = 28$. All 13 autosome pairs are represented by chromosome-level scaffolds (Fig. 1B). Haplotype 1 contains the X chromosome as an additional chromosome-level scaffold. Haplotype 2 contains the Y chromosome, which was assembled as several scaffolds. Overall, more than 96% of both haplotypes are contained in chromosome-level scaffolds (Fig. 1B). We estimated a very high base accuracy of QV (consensus quality) 64.2 and 64.5 for both haplotypes, indicating one error per ~2.6 million base pairs.

To systematically assess gene completeness among the *D. rotundus* and other available bat genomes, we applied TOGA (Tool to infer Orthologs from Genome Alignments), a method that infers orthologs from whole-genome alignments to 18,430 ancestral placental mammal-coding genes (Methods). In comparison to the Illumina *D. rotundus* assembly, the number of ancestral genes with missing sequences dropped from 1841 to 128 in our combined haplotype assemblies, whereas the number of genes with an intact reading frame increased from 15,295 to 17,301 (table S1). This indicates a substantially higher gene completeness in our assemblies, similar to the most contiguous bat assemblies generated to date (Fig. 1C) (25, 26).

A genome-wide screen revealed known and novel vampire bat-specific gene losses

To detect genes that were specifically lost in the vampire bat lineage, we used our two haplotype assemblies and considered 26 other bat

genomes (Fig. 1D and tables S1 and S2). Our screen included *Miconycteris hirsuta*, which represents the phylogenetically closest outgroup lineage to the clade that includes vampire bats and five other phyllostomid bats (*Artibeus jamaicensis*, *Carollia perspicillata*, *Anoura caudifer*, *Phyllostomus discolor*, and *Tonatia saurophila*) that represent sister lineages to vampire bats (Fig. 1D) (1). Using the human gene annotation as the reference, we applied TOGA to detect genes that exhibit gene-inactivating mutations (premature stop codons, frameshifts, splice site disruptions, and deletions of exons or entire genes) specifically in *D. rotundus*.

This screen revealed 13 vampire bat-specific gene losses. Three of these losses have been reported before: the sweet taste receptor gene *TAS1R2* and the bitter taste receptor genes *TAS2R5* and *TAS2R42* (20). These gene losses indicate a reduced sense of taste reception in vampire bats. To our knowledge, the remaining 10 gene losses [*REP15* (RAB15 effector protein), *FFAR1* (free fatty acid receptor 1), *SLC30A8* (solute carrier family 30 member 8), *PPP1R3E* (protein phosphatase 1 regulatory subunit 3E), *CTSE* (cathepsin E), *ERN2* (endoplasmic reticulum to nucleus signaling 2), *CTRL* (chymotrypsin like), *CYP39A1* (cytochrome P450 family 39 subfamily A member 1), *PDE6H* (phosphodiesterase 6H), and *RNASE7* (ribonuclease A family member 7)] have not been reported before.

The inactivating mutations in these 10 genes are displayed in Fig. 2A. In support of the validity of the underlying mutations, the 10 gene losses are also detected in the Illumina *D. rotundus* assembly and exhibit at least one shared inactivating mutation that is supported by both PacBio HiFi and Illumina reads. Further supporting gene loss, selection rate analysis showed that 9 of the 10 genes evolve under relaxed selection in *D. rotundus* to preserve the reading frame (significant for seven of nine genes; table S3). Last, inspecting publicly available *D. rotundus* RNA sequencing data, we either found no relevant expression in tissues where expression would be expected or found that the aligned reads supported the gene-inactivating mutations, indicating that potential transcripts cannot be translated into a full-length protein (fig. S2 and table S4).

As detailed below, the loss of these genes in the common vampire bat relates to a number of adaptations to their highly specialized blood diet, such as reduced insulin secretion and glycogen synthesis and a distinct stomach physiology (Fig. 2B). These gene losses further provide a possible mechanism contributing to vampire bats' exceptional social behavior and indicate the complete lack of cone photoreceptor function in *D. rotundus*.

Loss of *REP15* and enhanced iron excretion

The loss of *REP15*, a gene involved in regulating cellular iron uptake (27), is likely related to the obligatory iron-rich blood diet of vampire bats. Despite the importance of iron for various cellular processes, iron overload can have severe detrimental effects (12). The common vampire bat tolerates extreme dietary iron levels without exhibiting adverse effects (28); the relative amount of dietary iron was estimated to be 800-fold higher compared to humans (10). However, blood iron concentration in vampire bats has never been determined to our knowledge. Therefore, we measured whole-blood iron concentrations in wild-caught *D. rotundus* and compared it to two other neotropical bats (table S5). We found that blood iron content was significantly higher in the common vampire bat compared to the fruit-eating bat *Artibeus lituratus* [family Phyllostomidae; one-way analysis of variance (ANOVA) ($F = 4.24$, $P = 0.026$) and Tukey's post hoc tests: $P = 0.028$; Fig. 3A]. Vampire bats also had

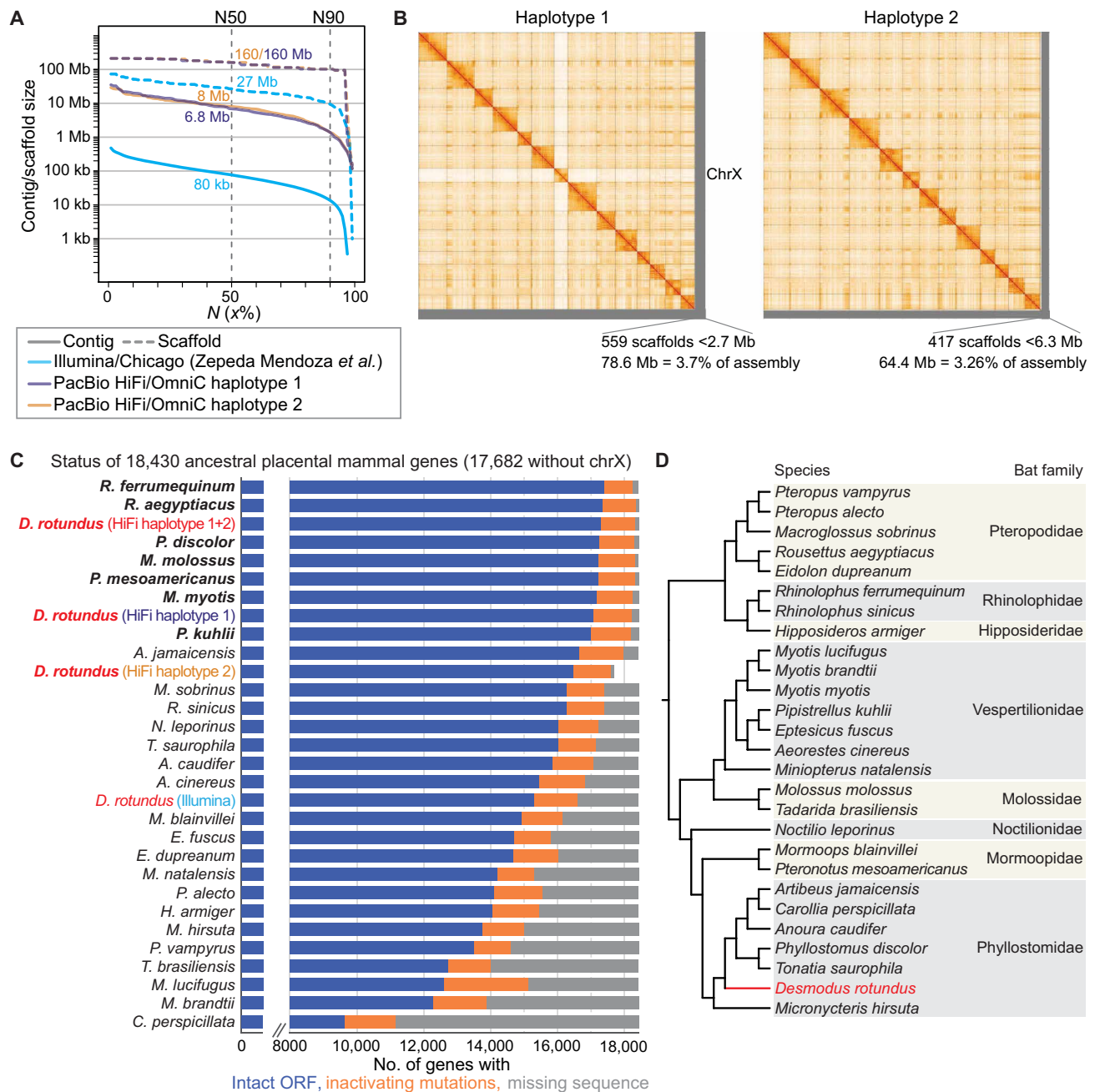


Fig. 1. Haplotype-resolved chromosome-level assembly of *D. rotundus*. (A) Comparison of assembly contiguity between our haplotype-resolved assemblies and the previous Illumina-based assembly (17). The graph shows contig (solid lines) and scaffold (dashed lines) sizes at the Y axis, for which x percent of the assembly consists of contigs and scaffolds of at least that size. (B) HiC contact maps show 14 and 13 chromosome-level scaffolds for haplotypes 1 and 2 that each comprise more than 96% of the respective haplotype assembly. Haplotype 1 contains the X chromosome. The Y chromosome is part of haplotype 2 and assembled into several shorter scaffolds. (C) Status of 18,430 ancestral placental mammal genes in each assembly, as inferred by TOGA. Genes are classified into those that have an intact reading frame (blue), have inactivating mutations (orange), or have missing coding parts due to assembly gaps or fragmentation (gray). Assemblies are sorted by the number of intact genes. Long read-based assemblies (bold font) consistently exhibit more intact genes and fewer missing genes compared to short read-based assemblies (not bold). For the *D. rotundus* haplotype 2 assembly that does not contain the X chromosome, we excluded genes located on the X chromosome and only considered the remaining 17,682 genes. To provide a fair comparison with previous assemblies that collapse both haplotypes, we also computed statistics for the union of both *D. rotundus* haplotype assemblies (haplotype 1+2), which exhibits the third highest number of intact genes of all included genomes. (D) Phylogeny of the bats analyzed in this study and the bat families they belong to (1).

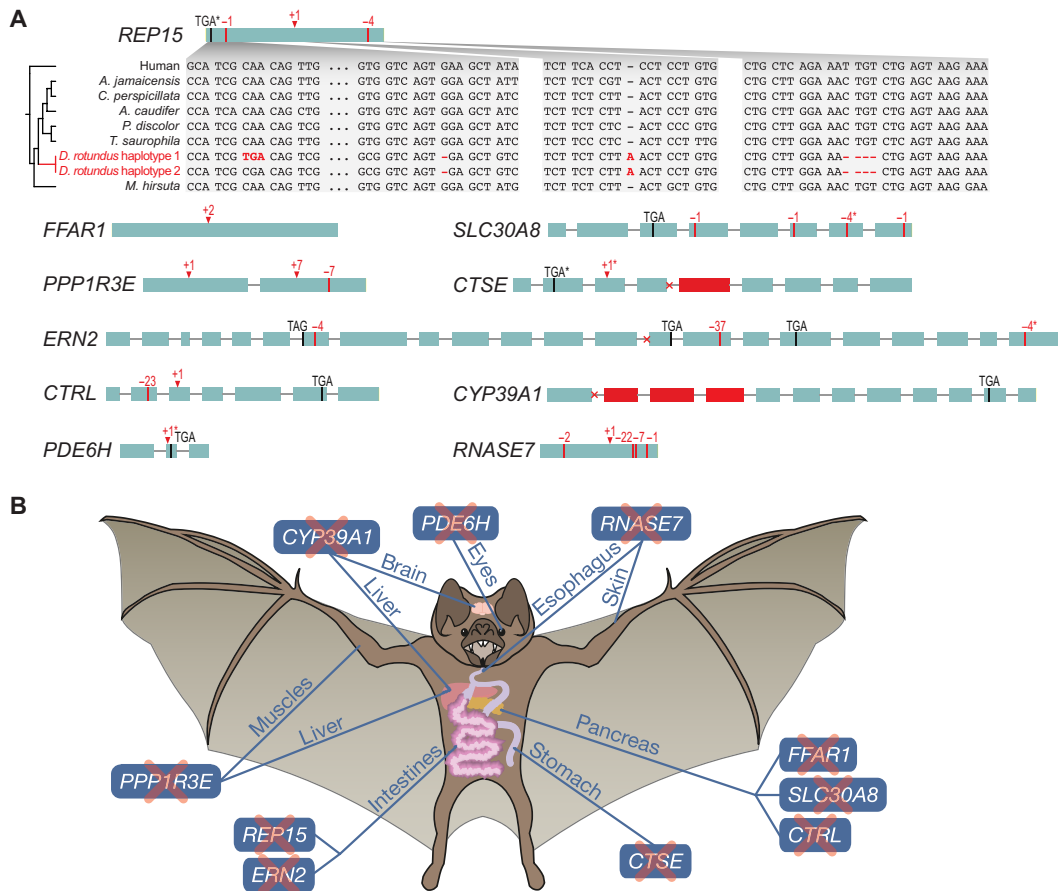


Fig. 2. Inactivating mutations and affected organ systems of 10 previously unknown vampire bat-specific gene losses. (A) Exon-intron structure visualization with inactivating mutations that were detected in the *D. rotundus* genome. Premature stop codons are shown as black vertical lines; frameshifting deletions are shown as red vertical lines, and frameshifting insertions are shown as red arrow heads. Donor or acceptor splice site mutations are indicated as a cross at the exon boundaries. Deleted exons are in red. Asterisks denote mutations that are heterozygous in our sequenced *D. rotundus* individual (present in only one of the two haplotype assemblies). The inset for *REP15* illustrates that inactivating mutations, and thus, gene loss was only detected in the common vampire bat. (B) Illustration of organs and anatomical sites where the 10 genes play important roles.

higher blood iron levels compared to the insectivorous outgroup bat *Myotis nigricans* (family Vespertilionidae; $P = 0.11$, not significant, likely because of the small sample size of four individuals; Fig. 3A). This suggests that vampire bats would benefit from mechanisms to lower systemic iron levels.

A 1980 study on the distribution of iron in the gastrointestinal tract revealed that *D. rotundus* uses iron excretion as one mechanism to reduce systemic iron levels (10). Specifically, this study identified large accumulations of iron in ferritin-containing vacuoles in *D. rotundus* gastrointestinal epithelial cells (Fig. 3B). Because the intestinal epithelium has a relatively fast turnover time (29), shedding iron-containing gastrointestinal cells into the intestinal lumen, as observed in *D. rotundus* (Fig. 3C) (10), eliminates iron from the body. Loss of *REP15* represents a plausible mechanism to enhance iron uptake in gastrointestinal cells and thus to boost iron excretion in *D. rotundus*.

REP15 is specifically expressed in the gastrointestinal tract (Fig. 4A) (30). Cellular overexpression of *REP15* decreases the amount of iron-transporting transferrin receptors on the cell surface (Fig. 4B) (27). Since transferrin receptor availability is a limiting factor for cellular iron uptake (31), the presence of *REP15* likely inhibits iron uptake from the bloodstream into gastrointestinal cells. Consistent

with this inhibitory effect, downregulation of *REP15* in colorectal cancer cells coincides with increased intracellular iron levels in these cells (32, 33). On the basis of these observations, it is expected that the loss of *REP15* in *D. rotundus* enhances iron accumulation in gastrointestinal tract cells, which matches the observation made by Morton and Wimsatt (10), and thus contributes to iron excretion.

In addition to enhanced excretion, a previous study found that vampire bats limit gastrointestinal iron absorption by increased expression of hepcidin, a factor that inhibits intestinal iron absorption (28). Furthermore, iron-storing ferritin genes are expanded in the common vampire bat genome (17), and these bats have high levels of iron-binding RFESD (Rieske Fe-S domain containing) in the serum proteome (34). Thus, limited iron absorption (mediated by increased hepcidin expression), a higher capacity for iron storage (mediated by ferritin and RFESD), and enhanced iron excretion (mediated by inactivating the inhibitory factor *REP15*) help vampire bats cope with their iron-rich diet.

Losses of *FFAR1* and *SLC30A8* and reduced insulin secretion

FFAR1 encodes a G protein-coupled receptor that is highly expressed in pancreatic β cells and senses medium- to long-chain free fatty acids (30, 35). Free fatty acids augment glucose-stimulated

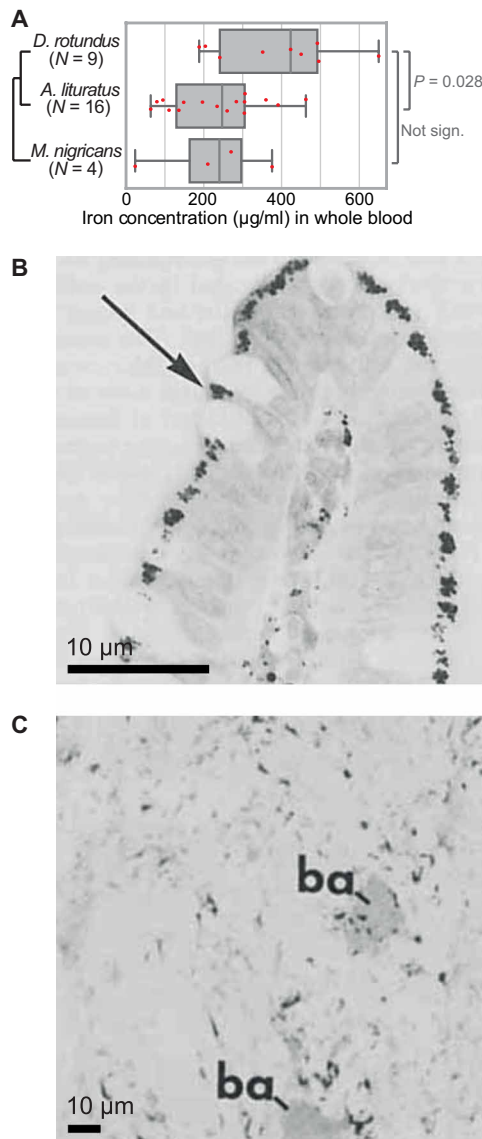


Fig. 3. Iron levels and iron excretion in *D. rotundus*. (A) Measurements of iron concentration in whole blood of *D. rotundus*, *A. lituratus*, and *M. nigricans* show that vampire bats have higher circulatory iron levels. *P* values are computed with one-way ANOVA and Tukey's post hoc tests. Two-sided *t* tests result in the same conclusions. (B) Light microscopy image, reproduced from figure 3 in (10), showing a longitudinal section of the upper villus half from the *D. rotundus* ileum. Prussian blue staining that indicates that iron demonstrates the presence of iron-containing cytoplasmic granules in epithelial cells (arrow). In addition to delivering iron via the bloodstream, a macrophage-linked mechanism contributes to iron deposition in these epithelial cells (10). (C) Prussian blue–positive granules are present in the forming feces of *D. rotundus*, showing that these bats excrete iron by shedding iron-containing intestinal cells. The figure is reproduced from figure 8 in (10).

insulin secretion, and *FFAR1* is a major factor that mediates this effect (Fig. 5) (35, 36). Glucose-stimulated insulin secretion involves an initial, rapid phase, which appears to be largely dependent on the depletion of an existing pool of membrane-docked insulin secretory granules, and a second, prolonged phase, which requires the production of new granules to supply the ongoing secretion process (35, 37). Deletion of *FFAR1* in mice reduces the amplifying

effect of free fatty acids in the prolonged phase by ~50% (36, 38). Consistent with this, *FFAR1* expression levels in human islets positively correlate with insulin secretion, which suggested that *FFAR1* deficiency could lower the insulin secretory capacities of β cells and thus contribute to the development of type 2 diabetes (39, 40). In addition to directly stimulating insulin secretion in β cells, *FFAR1* also amplifies insulin secretion indirectly (35). First, *FFAR1* is expressed in enteroendocrine cells, where its activation triggers the release of incretin hormones that stimulate pancreatic insulin secretion (41). Second, *FFAR1* is expressed in the brain and likely functions as a lipid sensor that influences insulin secretion through innervation of pancreatic islets (42). Hence, *FFAR1* amplifies insulin secretion via multiple mechanisms.

The free fatty acid sensor *FFAR1* likely became dispensable for vampire bats for two reasons. First, the *FFAR1* ligand (fatty acids) is barely present in their blood diet. Second, the low dietary sugar content likely abolishes the need for a normal glucose-stimulated insulin secretion, including the prolonged insulin secretion phase to which *FFAR1* substantially contributes. Vampire bats exhibit lower basal insulin levels than other mammals and show a substantially reduced insulin secretion with prolonged hyperglycemia upon an experimental glucose overload (9, 13). While having similarities to the defective insulin secretion response in human type 2 diabetes patients, in vampire bats, this is likely an adaptation to prevent hypoglycemia since glucose must remain in the bloodstream. Whereas a previous study detected signatures of positive selection in *FFAR1* and interpreted it as a means to improve glucose utilization in *D. rotundus* (17), our analysis reveals that *FFAR1* is actually lost and suggests that this gene loss relates to reduced insulin secretion under normal conditions and the inability to cope with high glucose intake when experimentally challenged. The loss of *FFAR1* in *D. rotundus* also provides an interesting contrast to fruit-eating bats of the phyllostomid and pteropodid families, which exhibit an increased capacity for insulin secretion and have convergently lost *FFAR3* (19, 22), a different β cell receptor that inhibits insulin secretion. This suggests that losses of two different genes with opposite effects on insulin secretion are involved in opposite phenotypes in bats.

SLC30A8 encodes the most highly expressed zinc transporter in pancreatic β cells (43, 44). In secretory granules of β cells, zinc is required for the formation of zinc-insulin hexamers (Fig. 5), which protect insulin from degradation (45, 46). Therefore, loss of the zinc transporter *SLC30A8* may have been a consequence of or may contribute to the decreased insulin secretion phenotype of *D. rotundus*.

Another not mutually exclusive hypothesis is that *SLC30A8* loss in vampire bats may be beneficial by reducing the requirements for body zinc levels. Although sufficient dietary zinc is available from mammalian blood (47), it might not be efficiently absorbed by vampire bats since high dietary iron concentrations can inhibit zinc absorption (48) and zinc, in turn, stimulates iron absorption in intestinal cells (49). Since blood has a high iron:zinc ratio of 66:1 (47), high dietary iron levels could induce zinc deficiency in vampire bats. *SLC30A8* knockout in mice causes extremely low zinc concentrations in β cells (50). Similarly, “natural *SLC30A8* knockouts” in mammalian herbivores such as guinea pig, sheep, and cow that also lost this gene are associated with low pancreatic islet zinc concentrations (51). Since β cells are normally among the cell types with the highest zinc concentration (52), it is possible that these herbivores may have lost *SLC30A8* because vegetarian diets are generally more

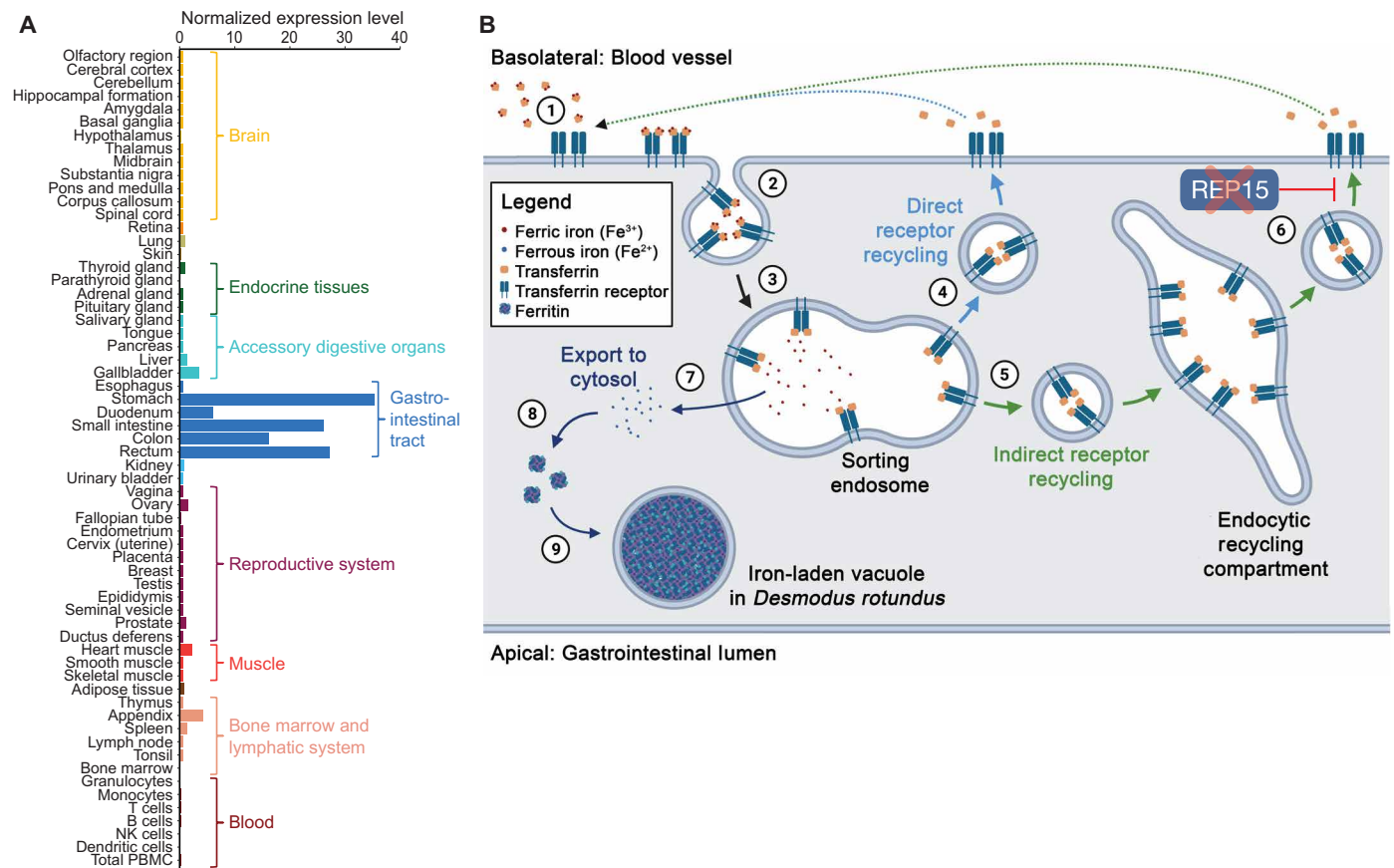


Fig. 4. Loss of *REP15* in *D. rotundus* and enhanced iron excretion. (A) *REP15* mRNA expression is highest in gastrointestinal tract tissues. Data were taken from the Human Protein Atlas (www.proteinatlas.org/ENSG00000174236-REP15/tissue) (30) and show the consensus RNA expression values that integrate three gene expression datasets. (B) Illustration of transferrin receptor–mediated cellular iron uptake and function of *REP15* in intestinal epithelial cells. Transferrin, an abundant ferric iron–binding plasma protein, binds to transferrin receptors that are present only in the basolateral membrane (1). Transferrin–transferrin receptor complexes are internalized via endocytosis (2). In sorting endosomes, ferric iron is released (3), and the unladen complexes are either directly targeted back to the cell membrane (4) or sent to the endocytic recycling compartment (5). *REP15*, encoded by the gene that is lost in *D. rotundus*, specifically localizes to the endocytic recycling compartment (6) and inhibits recycling of the unladen complex to the cell membrane (27), where transferrin and its receptor dissociate and the released transferrin can bind ferric iron again. Because the availability of transferrin receptors on the cell surface limits iron uptake (31), the presence of *REP15* normally inhibits cellular iron uptake. In the sorting endosome, ferric iron (Fe^{3+}) is reduced to ferrous iron (Fe^{2+}) and exported to the cytosol (7), where ferritin acts as the major high-capacity iron storage protein (8). Accumulations of ferritin and other “ferruginous” complexes enclosed in vacuoles (9) were observed in intestinal epithelial cells of *D. rotundus* (Fig. 3B). Loss of *REP15* likely enhances iron accumulation in intestinal epithelial cells, and shedding of these cells boosts iron excretion in *D. rotundus*.

limited in zinc content (53, 54). Repeated loss of *SLC30A8* in the vampire bat and in herbivorous mammals could therefore represent a strategy to restrict zinc utilization to other essential physiological functions. A precondition for this strategy would be that insulin stability and secretion does not depend on zinc anymore, as shown in guinea pigs, or that insulin secretion would not be essential anymore, as it seems to be the case for vampire bats.

Loss of *PPP1R3E* and impaired glycogen metabolism

PPP1R3E encodes a regulatory subunit of protein phosphatase 1 (PP1) (55). PP1 plays a central role in regulating a switch between synthesis and breakdown of glycogen, the major short-term storage form of glucose (56). By dephosphorylating glycogen synthase, PP1 activates this enzyme and promotes glycogen synthesis (57). By dephosphorylating glycogen phosphorylase, PP1 inhibits this enzyme and, consequently, glycogen breakdown (fig. S3A) (57). The activity of PP1 depends on a regulatory subunit, which is encoded by seven different genes with different expression patterns (*PPP1R3A*–

PPP1R3G) (55). These regulatory subunits are critical for PP1 activity, as overexpression of *PPP1R3A*, *PPP1R3B*, *PPP1R3C*, or *PPP1R3G* in cellular or animal models increases glycogen content, whereas their knockout reduces glycogen content (58–61). Although no animal studies of *PPP1R3E* exist, the gene is transcriptionally regulated by insulin, and *PPP1R3E* binds to glycogen (55). Thus, *PPP1R3E* most likely functions like the other glycogen-targeting subunits. With the exception of *PPP1R3E* loss in *D. rotundus*, none of the seven regulatory subunit–encoding genes exhibit inactivating mutations in any analyzed bat (fig. S3B).

The specific loss of *PPP1R3E* likely relates to the low glycogen concentrations in *D. rotundus* (14). Fed vampire bats have hepatic glycogen stores that are ~85% smaller than in fruit-eating bats and ~60% smaller than in other mammals fed on high-protein diets (14). Since sufficient glycogen stores are important to withstand periods of fasting, loss of *PPP1R3E* and the associated smaller glycogen stores may also contribute to the observed starvation vulnerability of vampire bats.

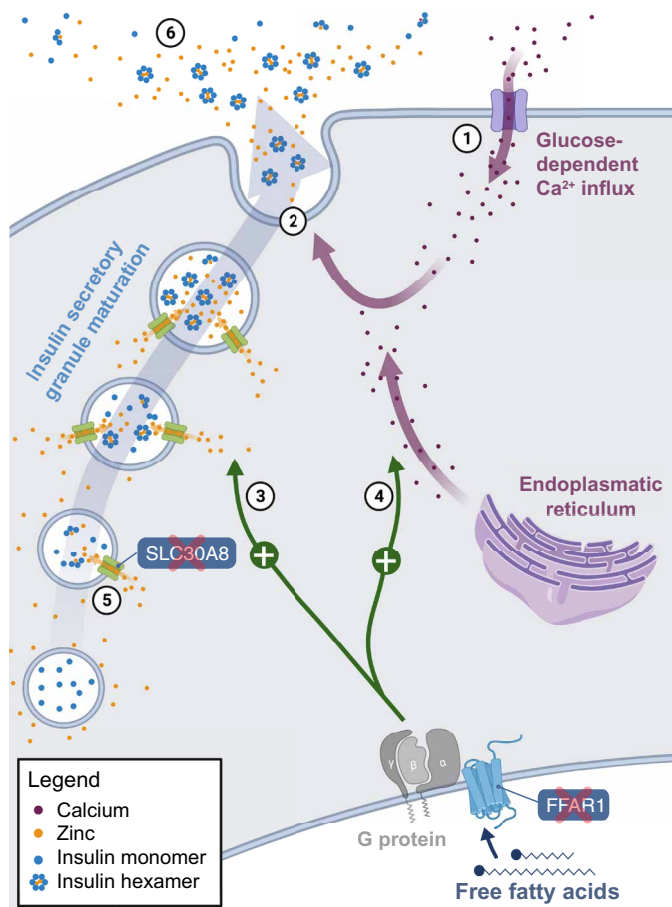


Fig. 5. Losses of *SLC30A8* and *FFAR1* in *D. rotundus* relate to reduced insulin secretion. Illustration of the roles of both genes in insulin synthesis and secretion in pancreatic β cells. Glucose-stimulated insulin secretion is initiated by the opening of voltage-gated calcium channels (1) (35). The resulting influx of calcium enhances insulin secretion by stimulating exocytosis of insulin secretory granules (2). *FFAR1* encodes a G protein–coupled receptor that, upon activation, enhances the prolonged insulin secretion phase via (F)-actin remodeling (3). *FFAR1* also triggers the release of calcium from the endoplasmic reticulum (4), which adds to the glucose-stimulated calcium influx and amplifies exocytosis of secretory granules. *SLC30A8* transports zinc into maturing insulin secretory granules, where zinc is essential for the formation of insulin hexamers (5). Upon secretion, these hexamers dissociate, releasing bioactive insulin monomers and zinc into the circulation (6). Loss of *FFAR1* and *SLC30A8* in *D. rotundus* is likely related to vampire bats' reduced insulin secretion.

Loss of *CTSE* and altered stomach function

The loss of *CTSE* in *D. rotundus* may be a consequence of extensive morphological and physiological modifications of their stomach, which is unparalleled by any other mammalian species (fig. S4). Most notably, the stomach of *D. rotundus* experienced fundamental remodeling from a compact muscular organ involved in mechanical and chemical digestion toward a distensible structure that functions primarily to store large amounts of ingested blood and serves as a major site of fluid absorption (fig. S4). *CTSE* is an intracellular protease that is highly expressed in gastrointestinal tissues, particularly in the stomach (30, 62). In the stomach, *CTSE* protein normally localizes to the canaliculi (invaginations) of parietal cells, which secrete hydrochloric acid, indicating that *CTSE* might be involved in secretory processes (63). In *D. rotundus*, the canaliculi of parietal

cells are specifically enriched in iron (10), suggesting that their gastric parietal cells experienced a functional shift from hydrochloric acid secretion toward participating in iron excretion, which could have rendered *CTSE* dispensable. Consistent with this, *CTSE* has been reported lost in platypus (64), which lacks an acid-secreting stomach. However, *CTSE* is also lost in *Cetartiodactyla*, which have acid-secreting stomachs (65), and in addition to a possible role in gastric acid secretion, *CTSE* also has immune-related functions (62). Thus, other *CTSE* functions could have also contributed to or represent the primary reason of *CTSE* loss in *D. rotundus*.

Loss of *ERN2* and low dietary fat content

The loss of *ERN2* in *D. rotundus* is likely a consequence of the low fat content of their blood diet. *ERN2* is specifically expressed in gastrointestinal epithelia (66) and encodes a transmembrane protein that inhibits the production of chylomicrons, which are lipoprotein particles that transport dietary lipids absorbed in enterocytes to other tissues (67, 68). Enterocytes of *ERN2* knockout mice were shown to secrete more chylomicrons, resulting in increased lipid absorption and a more pronounced hyperlipidemia on high-fat diets (67, 68). On a standard diet, *ERN2* knockout mice did not exhibit hyperlipidemia, indicating that *ERN2* limits intestinal lipid absorption only under conditions where excessive fat is available. Since blood has a very low fat content (9), it is conceivable that regulatory mechanisms, which normally limit lipid absorption, became dispensable during vampire bat evolution, resulting in loss of *ERN2*.

Loss of the pancreatic chymotrypsin *CTRL*

Pancreatic proteases such as chymotrypsinogens and trypsinogens are among the most essential digestive enzymes (69). They are produced by acinar cells of the exocrine pancreas and are secreted as inactive zymogens, which, upon activation in the small intestine, digest proteins (69). *CTRL* encodes one of four chymotrypsinogen isoforms and is considered a predictive biomarker for human pancreatic cancer (70). In mice, *CTRL* represents a minor chymotrypsin isoform, constituting ~10% of the chymotrypsinogen pool (71). In vitro experiments showed that *CTRL* cleaves trypsinogens and thus inhibits the activation of protein-digesting trypsin (71). Consistently, *CTRL* knockout in mice leads to a reduced activation of chymotrypsins and a slightly higher trypsin activity (71), which could be relevant for the unique, protein-rich diet of vampire bats. Recent evidence also indicates that acinar proteases including *CTRL* contribute to the proliferation of β cells (72), providing another possible explanation for the loss of this gene in a bat species that exhibits a reduced β cell mass (13).

Loss of *CYP39A1* and advanced social behavior

The loss of *CYP39A1* could have contributed to the evolution of vampire bats' exceptional social behaviors and cognitive abilities (16, 73, 74). *CYP39A1* encodes an oxysterol 7- α -hydroxylase enzyme (75). This enzyme is expressed in the liver but contributes only a small portion to the total hepatic bile acid synthesis (fig. S5). In addition, *CYP39A1* is expressed in the brain, where it is the only expressed enzyme that can degrade the cholesterol metabolite 24S-hydroxycholesterol (76–79). In the brain, 24S-hydroxycholesterol is produced from cholesterol by the brain-specific enzyme *CYP46A1* and represents a metabolite during cholesterol elimination from the brain (80). Unlike cholesterol, 24S-hydroxycholesterol can pass the blood-brain barrier (81). Therefore, the loss of the 24S-hydroxycholesterol-degrading *CYP39A1* is expected to result in elevated systemic levels

of this metabolite, which was observed in humans with *CYP39A1* loss-of-function alleles (82).

Since 24S-hydroxycholesterol also plays important neurophysiological roles, we hypothesize that increased levels of 24S-hydroxycholesterol, mediated by *CYP39A1* loss, may be connected to the exceptional cognitive and social capabilities of *D. rotundus*. 24S-hydroxycholesterol is a potent, allosteric and direct activator of *N*-methyl-D-aspartate receptors (NMDARs) (83, 84), which are glutamate-gated ion channels that mediate synaptic plasticity and memory formation. In the hippocampus, 24S-hydroxycholesterol lowered the stimulus threshold required for the induction of long-term potentiation (83), one of the major mechanisms for learning and memory. Increased cerebral 24S-hydroxycholesterol levels (mediated by overexpressing the 24S-hydroxycholesterol-synthesizing enzyme *CYP46A1*) improve spatial memory function in mice (85), whereas reduced 24S-hydroxycholesterol levels (mediated by deleting *CYP46A1*) cause deficiencies in hippocampal long-term potentiation and impaired learning and memory function (86). Consistent with 24S-hydroxycholesterol exerting a direct effect on NMDAR activity and cognitive function, administration of 24S-hydroxycholesterol analogs reversed an induced reduction in synaptic NMDAR frequency and function, long-term potentiation, and memory formation in mice (87). NMDAR activity also exerts a strong influence on social behavior, as NMDAR agonists improve social behavior in rodents, whereas antagonists impair it (88). Thus, while genetic perturbation studies of *CYP39A1* do not yet exist, it is plausible that *CYP39A1* inactivation in *D. rotundus* increases 24S-hydroxycholesterol levels, as observed in human, which may have a positive effect on social behavior and cognitive abilities.

Vampire bats, the only lineage in our dataset that lost the 24S-hydroxycholesterol-metabolizing *CYP39A1* gene (fig. S5), are distinguished from other bats by their exceptional social behavior and cognitive abilities. They reciprocally share regurgitated blood with roost mates that failed to obtain a nightly meal and would otherwise face starvation (16). The decision with whom to share blood is primarily driven by recognizing contact calls of individuals that provided past blood donations, which demonstrates exceptional long-term social memory (16, 73). Furthermore, nonkin adoption of orphaned offspring occurs in vampire bat colonies (74). Vampire bats also form long-lasting social bonds, evident by observations that individuals who cooperated in captivity retain their social network when released into the wild (89). Vampire bats, as perhaps the most socially advanced bats, were also found to have the largest relative neocortical volume among 276 measured bat species (90). The 24S-hydroxycholesterol-interacting subunit of NMDAR [glutamate ionotropic receptor NMDA type subunit 2B (*GluN2B*) encoded by *GRIN2B*] is highly expressed in the cortex during late embryogenesis and at birth (91, 92) and plays an important role in cortical development (84, 93). This raises the possibility that *CYP39A1* loss may also be connected to the large neocortical volume of *D. rotundus*, which could be explored in future studies.

Loss of cone phototransduction genes suggests rod monochromacy

Our strict genomic screen revealed that *PDE6H* is exclusively lost in vampire bats. *PDE6H* encodes the γ subunit of the cone phosphodiesterase, a component of the phototransduction cascade in cone cells (94). Loss-of-function mutations in *PDE6H* cause total color blindness in humans (94), but not in mice, where the rod phosphodiesterase isoform *PDE6G* compensates for *PDE6H* loss (95). Given

this cross-species variability, we investigated additional genes required for phototransduction in rods and cones in the 27 focal bat species. For rods, we found no phototransduction component (*RHO*, *GNAT1*, *GNB1*, *GNGT1*, *PDE6A*, *PDE6B*, and *PDE6G*) to be lost. Among the genes required for cone phototransduction (*OPN1SW*, *OPN1LW*, *GNAT2*, *GNB3*, *GNGT2*, and *PDE6C*), we confirmed previously reported losses of the short wavelength-sensitive opsin (*OPN1SW*) in the vampire bat and six other bats (fig. S6). In addition, our analysis detected that *PDE6C* is lost in the vampire and four other bats (figs. S6 and S7). Inactivating mutations in *PDE6C* in both humans and mice abolish cone function entirely, resulting in rod monochromacy, a condition where only rod photoreceptors remain functional (96, 97).

While ancestral Chiroptera were inferred to have two types of cones and dichromatic vision, many bats, including *D. rotundus*, lack cones that express a functional short wavelength-sensitive opsin (*OPN1SW*) (fig. S6). Whereas the lack of a functional *OPN1SW* alone suggested color blindness but maintenance of functional cones expressing the conserved *OPN1LW* (long wave-sensitive opsin) gene, our discovery of repeated *PDE6C* losses suggests that *D. rotundus* and four other nocturnal Noctilionoidea may be functional rod monochromats. This condition, where all cone-based photoreception is abolished even if vestigial cone cells can still be detected, has been suggested for only a few other mammalian lineages so far (98). In light of their ecology, rod monochromacy is plausible in vampire bats, which lost both *PDE6C* and *PDE6H*. These strictly nocturnal bats are most active during the darkest periods of the night and even avoid moonshine. Furthermore, to locate their prey, vampire bats have evolved nonvisual sensory adaptations such as highly specialized auditory adaptations (99) and an infrared sensing capability, which is unique among mammals (5).

Loss of the immune-related *RNASE7* and a different pathogen profile of blood

Feeding exclusively on blood, the immune system of vampire bats is regularly challenged with blood-borne pathogens (100). However, because blood exhibits a low bacterial abundance but different species composition (101), it is possible that their intestinal tract is exposed to a different diversity of pathogens. We found that the immune-related *RNASE7* gene is lost in *D. rotundus* and intact in all other analyzed bats.

RNASE7 encodes a secreted ribonuclease that has potent antimicrobial activity against various microorganisms (102). In humans, *RNASE7* is highly expressed in most epithelia, including skin, urothelium, and respiratory tract epithelium (30, 102). The gene is significantly downregulated in the skin and urinary tract of diabetic patients (potentially because *RNASE7* expression can be induced by insulin signaling), which reduces innate immune defense capacities and likely contributes to the much higher incidence of bacterial skin and urinary tract infections in diabetic patients (103, 104). The exclusive loss of *RNASE7* in vampire bats, which might also be related to their reduced insulin secretory capacities, raises the question of whether epithelial tissues of vampire bats have a reduced capacity for secreting bactericidal peptides. While a previous study found that *RNASE7* evolved under positive selection in vampire bats, which was interpreted as an adaptation toward increased exposition to blood-borne pathogens (17), our analysis shows that *RNASE7* is clearly inactivated, which raises the possibility that its loss may be a consequence of exposure to a different pathogen diversity.

Summary

We used long read (HiFi) sequencing to generate a haplotype-resolved genome assembly of high completeness, contiguity, and base accuracy for the common vampire bat *D. rotundus*. Adding to previous studies (25), our side-by-side comparison of gene content and inactivating mutations demonstrates that the HiFi assembly improves not only gene completeness but also base accuracy. A haplotype-resolved assembly also facilitates discriminating between homozygous and heterozygous (inactivating) mutations, which is more difficult in collapsed diploid assemblies. Using this new *D. rotundus* assembly and existing genomes of 26 other bats, we performed a genome-wide screen for genes that are specifically lost in the vampire bat lineage. This screen revealed 10 previously unknown gene losses that are likely associated with derived phenotypic features of vampire bats, such as reduced insulin secretion (*FFAR1* and *SLC30A8*) and glycogen synthesis (*PPP1R3E*) and a distinct gastric physiology (*CTSE*). The loss of *CYP39A1* is expected to result in elevated 24S-hydroxycholesterol levels and could be linked to the exceptional social behavior and cognitive abilities of *D. rotundus*. The loss of other genes (*ERN2*, *CTRL*, and *REP15*) is likely related to the biased nutrient composition of blood, which features low fat, high protein, and high iron contents. Consistent with an association with vampire bat-specific changes in metabolism and digestion, many of these genes are highly expressed in relevant organ systems such as the pancreas (*FFAR1*, *SLC30A8*, and *CTRL*) and gastrointestinal tissues (*REP15*, *CTSE*, and *ERN2*). Last, gene loss can also indicate previously unknown phenotypes, exemplified here by the loss of *PDE6H* and *PDE6C*, which suggest the complete lack of cone photoreceptor function (functional rod monochromacy). Similarly, the loss of *RNASE7* may indicate differences in the immune system between *D. rotundus* and other bats, which deserves further studies. In particular, it is not known whether *D. rotundus* is exposed to a distinct pathogen profile, largely constrained to blood-borne pathogens. This could be investigated with metagenomic approaches (105) to systematically characterize and compare pathogen profiles of vampire and other bats, ideally in matched environments.

Which genes are lost during the course of evolution is influenced by several factors. One important factor underlying gene loss, including those identified here, is the absence of selection to preserve the function of certain genes as a consequence of adaptation to a new environment or different lifestyle. However, despite dispensability of gene function, several other factors constrain which genes are permitted to be lost in evolution (21). For example, genes lost in mammals are generally depleted in essential functions and tend to have a lower degree of pleiotropy (65). The few known examples of pleiotropic gene losses in mammals refer to cases where most or all functions of the gene became dispensable [e.g., *KLK8*, *INSL5*, *RXFP4*, and *SLC4A9* (23, 24, 106)] or where additional gene functions are compensated by functionally related proteins [e.g., *ACOX2* and *SLC27A5* (107)]. Consistent with pleiotropy being a key restricting factor, the gene loss cases detected here largely refer to genes with specific functions and a low or no degree of pleiotropy. In addition to pleiotropy and essentiality, restricted expression patterns appear to be another factor permitting gene loss. For example, while the inactivated gene *ERN2* exhibits a specific expression in the gastrointestinal tract, the ubiquitously expressed and functionally similar *ERN1* gene (66) is intact in the vampire bat genome. Similarly, *REP15*, *SLC30A8*, *CTSE*, and *CTRL* have tissue-restricted expression patterns.

While dispensability of gene function is certainly the main explanation for gene losses in the vampire bat lineage, loss of ancestral genes can sometimes be beneficial in evolution and contribute to adaptations (21–24). For example, the loss of *REP15* could contribute to enhanced iron elimination through shedding of iron-containing gastrointestinal cells, which likely represents an adaptation of vampire bats to their iron-rich blood diet. Another example is *CYP39A1*, whose loss is expected to result in elevated systemic levels of 24S-hydroxycholesterol. Since elevated levels of this cholesterol metabolite can positively affect cognitive function in animal models (85, 108), it is conceivable that loss of *CYP39A1* in the vampire bat lineage may have contributed to their exceptional social behavior and cognitive abilities, which is a unique feature among bats.

In summary, our study provides novel insights into the genomic changes related to adaptations to sanguivory and the evolutionary importance of gene loss in general. Notably, a comprehensive understanding of how sanguivory as a unique dietary specialization has evolved requires not only high-quality genomic resources but also data on the organismal biology of vampire bats. Our study reveals gaps in our knowledge of vampire bat physiology, metabolism, and immunity, highlighting the need to better characterize the phenotypic side of adaptations to their unique diet.

METHODS

All software and tools with the version number and references are listed in table S6.

Sample collection for sequencing

A *D. rotundus* male individual (ROMM126221) was collected in a mist net at Sabajo, Para, Suriname on 26 September 2017 as part of a larger environmental baseline study and euthanized with an overdose of isoflurane. The research permit was approved on 8 June 2017 by the Nature Conservation Division, Suriname Forest Service. Animal Use Protocol #2017-19 was approved by the Animal Care Committee of the Royal Ontario Museum. The use of wild mammals in research followed the guidelines of the American Society of Mammalogists.

DNA extraction, library preparation, and whole-genome sequencing

Sampled tissues were snap-frozen in liquid nitrogen immediately after dissection and stored at -80°C until further processed. Mixed tissue of heart, liver, and spleen (23 mg) was used for high molecular weight DNA extraction using the Nanobind Tissue Big DNA Kit (Circulomics, MD) according to the manufacturer's instructions. Final DNA purity and concentrations were measured using NanoPhotometer (Implen GmbH, Munich, Germany) and Qubit Fluorometer (Thermo Fisher Scientific, Waltham, MA). Two SMRTbell libraries were constructed following the instructions of the SMRTbell Express Prep Kit v2.0 (Pacific Biosciences, Menlo Park, CA). The total input DNA for each library was approximately 5 μg . The libraries were loaded at an on-plate concentration of 80 pM using diffusion loading. Four SMRT cell sequencing runs were performed on the Sequel System IIe in CCS mode using 30-hour movie time with 2 hours of pre-extension and sequencing chemistry V2.0. The Dovetail Omni-C library was prepared from mixed tissue (heart, liver, and spleen) using the Dovetail Omni-C kit (Dovetail Genomics, Scotts Valley, CA, USA) following the manufacturer's protocol

(manual version 1.2 for mammalian samples). The Omni-C library was sequenced on a NovaSeq 6000 platform at Novogene (UK), generating 400 million 2×150 bp paired-end reads totaling 120 Gbp. The fragment size distribution and concentration of the final PacBio and Dovetail Omni-C library were assessed using a TapeStation (Agilent Technologies) and a Qubit Fluorometer (Thermo Fisher Scientific, Waltham, MA), respectively.

D. rotundus genome assembly

We called CCS reads ($rq > 0.99$) from the subreads.bam file using PacBio ccs. We then created the two contig assemblies using hifiasm with arguments `-l2 --h1 --h2` using the CCS reads and the HiC reads as input. This resulted in one contig assembly for each of the haplotypes in this species, which both went independently into the following scaffolding, gap-closing, and polishing steps.

For scaffolding, we used SALSA2 and the Dovetail Omni-C mapping pipeline. Briefly, we mapped HiC reads using BWA-MEM. Alignments were filtered using pairtools with arguments `parse --min-mapq 40 --walks-policy 5unique --max-inter-align-gap 30` to retain those alignments with high mapping quality, the most 5' alignments for conflicts, and alignments without large gaps. We removed potential polymerase chain reaction duplicates using pairtools dedup. The resulting read-sorted bed file was used as input for SALSA2. We then performed a number of manual curation rounds to correct scaffolding errors and to scaffold those contigs that were not automatically scaffolded. To this end, we used cooler and HiGlass to visually inspect the HiC maps and rescaffolded the assembly using SeqKit to rearrange contigs and scaffolds into chromosome-level scaffolds.

After scaffolding, we closed additional assembly gaps using the lower-quality PacBio CLR read data that did not yield a CCS read. To this end, we mapped the original subreads.bam files to the scaffolded assembly using pbmm2 with arguments `--preset SUB-READ -N 1`. On the basis of the read-piles created by reads spanning across gap regions, we computed consensus sequences for the gap regions and their 2-kb up/downstream flanks using gcpp. We filtered for high-confidence consensus sequences by requiring that no N's and no lowercase (acgt) characters remain in the consensus sequence. We then replaced the assembly gap and flanking region with high-confidence consensus sequences.

Despite the high accuracy of PacBio CCS reads, an assembly can still contain base errors due to errors in the consensus sequence calculation. In addition, lower base accuracy likely exists in the closed gap regions. To improve base accuracy, we polished both haplotype assemblies using all CCS reads. We tested both freebayes and DeepVariant. On the basis of numbers of genes with inactivating mutations (computed by TOGA, see below) and the QV values computed by Merqury, DeepVariant vastly outperformed freebayes in correcting base errors. Therefore, for the final polishing round, we mapped all CCS reads to the scaffolded, gap-closed assemblies using pbmm2 with arguments `--preset CCS -N 1` and called variants using DeepVariant. We then filtered for sites with "genotype 1/1" to specify that all or nearly all reads support an alternative sequence at this position and a "PASS" filter value to specify that the site passed DeepVariant's internal filters. We then corrected base errors using bcftools consensus (version 1.12). This procedure does not "correct" any heterozygous or polymorphic regions but only those that are incorrect and not supported by any CCS reads.

Repeat masking

We used RepeatModeler (parameter `-engine ncbi`) to generate a de novo repeat library for the new *D. rotundus* genome assembly and used the resulting library with RepeatMasker (parameters `-engine crossmatch -s`) to soft-mask the genome.

Genome alignments

We used the human hg38 genome assembly as the reference and considered *D. rotundus* and 26 other bats as query species (Fig. 1D). Table S1 lists the species with their taxonomic lineage, the genome assembly accessions, and contig/scaffold N50 values. To generate pairwise genome alignment chains as input for TOGA, we first used LASTZ with parameters ($K = 2400$, $L = 3000$, $Y = 9400$, $H = 2000$, and the LASTZ default scoring matrix). These parameters are sensitive enough to capture orthologous exons between placental mammals (109). Then, we used axChain (default parameters except `linear-gap = loose`) to compute colinear alignment chains, RepeatFiller (default parameters) to capture previously missed alignments between repetitive regions, and chainCleaner (default parameters except `minBrokenChainScore = 75,000` and `-doPairs`) to improve alignment specificity.

Using TOGA to infer orthologous genes and detect gene losses

To compare gene completeness and to screen for gene losses, we used TOGA, a method that uses pairwise genome alignment chains between an annotated reference genome (here, human hg38 assembly) and other query species. Briefly, TOGA uses machine learning to infer orthologous loci for each reference transcript, utilizing that orthologous genes display more alignments between intronic and flanking intergenic regions. TOGA then projects each reference transcript to its orthologous query locus using CESAR 2.0, a Hidden Markov model method that takes reading frame and splice site annotation of the reference exons into account. CESAR avoids spurious frameshifts and is able to detect evolutionary splice site shifts and precise intron deletions. Using the CESAR alignment, TOGA determines whether the transcript has inactivating mutations (frameshifting mutations, premature stop codons, splice site disrupting mutations, and deletions of entire coding exons). TOGA also uses orthologous alignment chains to detect genes that are entirely deleted in the query assembly and distinguishes real exon or gene deletions from missing sequence caused by assembly gaps.

TOGA classifies each transcript into one of five categories. Classifications "intact," "partially intact," and "missing" refer to transcripts that lack inactivating mutations in the middle 80% of the coding region. TOGA specifically considers this central part of the coding region since truly conserved genes can have inactivating mutations in the first or last 10% of the coding region (near the N or C terminus) (110). For intact transcripts, the central part of the coding region is completely present in the assembly, whereas for partially intact ($\geq 50\%$ present) and missing ($< 50\%$ present) transcripts, some coding parts are missing because of assembly gaps or fragmentation. Classification "lost" refers to transcripts that have at least two inactivating mutations in at least two exons. All other transcripts, having a single inactivating mutation or mutations in only a single exon, are classified as "uncertain loss," reflecting the possibility that only an exon but not the entire gene could be lost.

Considering all input transcripts of a gene, TOGA uses the precedence order "intact, partially intact, uncertain loss, lost, and

missing” to provide a gene classification. That means TOGA only classifies a gene as lost if all its transcripts are classified as lost (at all orthologous loci, if there is more than one).

Gene completeness among bat genomes

To compare gene completeness between assemblies, we first obtained a set of genes that likely already existed in the placental mammal ancestor. To this end, we used the human GENCODE V38 (Ensembl 104; www.gencodegenes.org/) gene annotation as input and applied TOGA to the genomes of 11 afrotherian (represented by aardvark, cape golden mole, small Madagascar hedgehog, Talazac’s shrew tenrec, cape elephant shrew, dugong, manatee, Asiatic elephant, African savanna elephant, cape rock hyrax, and yellow-spotted hyrax) and 5 xenarthran (represented by southern two-toed sloth, Hoffmann’s two-fingered sloth, nine-banded armadillo, giant anteater, and southern tamandua) mammals. Since each input gene is, by definition, present in human (superorder Boreoeutheria), we considered a gene as ancestral if it is also conserved in the other two basal placental superorders Afrotheria and Xenarthra. Specifically, we selected genes that are classified by TOGA as intact or partially intact in at least one afrotherian and at least one xenarthran genome. Note that this requirement assures placental mammal ancestry irrespective of the exact basal split of placental mammals, which is difficult to resolve. This procedure resulted in a set of 18,430 genes.

Next, we applied TOGA to *D. rotundus* and the 26 other bat genomes (table S1). Considering the 18,430 ancestral genes, we counted per species how many genes have an intact reading frame (TOGA classification intact), have inactivating mutations (TOGA classifications loss and uncertain loss), or have missing sequence (TOGA classifications partially intact and missing). This breakdown is shown in Fig. 1C.

Screen for gene losses

To identify gene losses that, among bats, occurred specifically in the vampire bat lineage, we used the above-generated TOGA data for the 27 bats. We first filtered for genes that have at least one inactivating mutation in the middle 80% of the coding sequence (TOGA classification lost or uncertain loss) in both *D. rotundus* haplotype assemblies.

Base errors can also occur in other bat assemblies, which may result in missing real vampire bat–specific gene losses (false negatives). To reduce the false negative rate, we conducted the initial screen with less strict requirements and allowed per gene up to three non–vampire bat species to be classified as missing, partially missing, or uncertain loss, resulting in 52 candidate genes. Then, to assess which of these candidate genes are true vampire-specific gene losses, we mapped available Illumina reads of the same species to each included genome assembly using BWA-MEM and removed duplicates with Picard (Sequence Read Archive identifiers are listed in table S2) and examined whether putative inactivating mutations are supported by raw reads and if they are heterozygous or homozygous. We excluded all genes as non–vampire–specific losses that have homozygous mutations in at least one other bat species and furthermore required that not more than 60% of the coding sequence remains functional in *D. rotundus*. We kept *SLC30A8*, which has a heterozygous stop codon in exon 4 in *M. hirsuta*. We excluded genes belonging to the large and fast-evolving olfactory receptor family. This procedure revealed the 13 vampire-specific gene losses that are discussed here.

Last, to confirm the correctness of all 10 previously unknown vampire bat–specific gene losses, we manually inspected the pairwise alignment chains in the UCSC genome browser, which showed that the remnants of all 10 genes are located in a conserved gene order (synteny) context. Inspecting chiropteran pairwise alignment chains also showed that none of the 10 genes exhibit duplications in *D. rotundus* or other bats, which excludes the possibility that a functional gene copy remained in *D. rotundus*. Last, we further verified the correctness of the inactivating mutations by requiring that the gene is also classified as lost or uncertain loss in the Illumina *D. rotundus* assembly with at least one shared homozygous (based on aligned Illumina sequencing reads) inactivating mutation, thus providing base support from two sequencing technologies.

Relaxed selection

To test the 10 genes for relaxation of selection, we obtained pairwise codon alignments between human and each query bat from TOGA. Codons affected by frameshifting insertions or deletions and premature stop codons were replaced by “NNN” codons to maintain a reading frame. A multiple codon alignment was produced with MACSE v2 and cleaned with HmmCleaner with default cost values. The resulting alignments were used to investigate whether the gene evolves under relaxed selection with RELAX, specifying the *D. rotundus* branch as the foreground and all other branches as background.

Publicly available gene expression data

We investigated RNA expression of the 10 target gene losses using publicly available transcriptome sequencing data for *D. rotundus* from 11 tissues (heart, stomach, intestine, liver, gallbladder, pancreas, spleen, kidney, olfactory epithelium, eye, and tongue). The paired-end sequencing read sets were downloaded from NCBI (accessions are listed in table S4) and mapped to the new *D. rotundus* haplotype 1 assembly using STAR. Target loci were then manually examined in IGV (integrative genomics viewer).

Whole-blood iron measurements

Nine *D. rotundus*, 16 *A. lituratus*, and 4 *M. nigricans* individuals were captured with mist nets in Viçosa, Minas Gerais, Brazil. Following euthanasia, blood samples were collected in the field. As the results were expressed as microgram per milliliter, we measured each sample volume in the field, which varied between 100 and 400 μ l. Tubes were kept on ice until storage at -20°C in the laboratory for a maximum of 1 month. For iron level measurements, all blood samples were dried using a stove and mineralized in a nitric-perchloric acid solution (total volume, 1.5 ml) until organic matter was removed. The final extract was used to determine iron concentrations through atomic absorption spectrophotometry (Shimadzu, AA-6701F) (table S5). All animal captures were approved by the National Environmental Office (license number 77322-1; Sisbio, Brazil), and all experiments were approved by the Ethics Committee from Federal University of Viçosa (license number 10/2021; CEUA/UFV, Brazil).

Statistical analysis

Whole-blood iron levels were compared between species using one-way ANOVA and Tukey’s post hoc testing, as well as with two-sided *t* tests with the SciPy stats library.

SUPPLEMENTARY MATERIALS

Supplementary material for this article is available at <https://science.org/doi/10.1126/sciadv.abm6494>

[View/request a protocol for this paper from Bio-protocol.](#)

REFERENCES AND NOTES

- R. J. Baker, O. R. P. Bininda-Emonds, H. Mantilla-Meluk, C. A. Porter, R. A. Van Den Bussche, Molecular time scale of diversification of feeding strategy and morphology in New World leaf-nosed bats (Phyllostomidae): A phylogenetic perspective, in *Evolutionary History of Bats: Fossils, Molecules and Morphology*, G. F. Gunnell, N. B. Simmons, Eds. (Cambridge University Press, 2012), pp. 385–409.
- U. Schmidt, Orientation and sensory functions in *Desmodus rotundus*, in *Natural History of Vampire Bats* (CRC Press, 2018), pp. 24.
- U. Schmidt, Olfactory threshold and odour discrimination of the vampire bat (*Desmodus rotundus*). *Period Biol* **75**, 89–92 (1973).
- R. S. Heffner, G. Koay, H. E. Heffner, Hearing in American leaf-nosed bats. IV: The common vampire bat, *Desmodus rotundus*. *Hear. Res.* **296**, 42–50 (2013).
- E. O. Gracheva, J. F. Cordero-Morales, J. A. González-Carcacia, N. T. Ingolia, C. Manno, C. I. Aranguren, J. S. Weissman, D. Julius, Ganglion-specific splicing of TRPV1 underlies infrared sensation in vampire bats. *Nature* **476**, 88–91 (2011).
- D. K. Riskin, S. Parsons, W. A. Schutt Jr., G. G. Carter, J. W. Hermanson, Terrestrial locomotion of the New Zealand short-tailed bat *Mystacina tuberculata* and the common vampire bat *Desmodus rotundus*. *J. Exp. Biol.* **209**, 1725–1736 (2006).
- J. S. Davis, C. W. Nicolay, S. H. Williams, A comparative study of incisor procumbency and mandibular morphology in vampire bats. *J. Morphol.* **271**, 853–862 (2010).
- D. H. Low, K. Sunagar, E. A. B. Undheim, S. A. Ali, A. C. Alagon, T. Ruder, T. N. W. Jackson, S. P. Gonzalez, G. F. King, A. Jones, A. Antunes, B. G. Fry, Dracula's children: Molecular evolution of vampire bat venom. *J. Proteomics* **89**, 95–111 (2013).
- C. P. Breidenstein, Digestion and assimilation of bovine blood by a vampire bat (*Desmodus rotundus*). *J. Mammal.* **63**, 482–484 (1982).
- D. Morton, W. A. Wimsatt, Distribution of iron in the gastrointestinal tract of the common vampire bat: Evidence for macrophage-linked iron clearance. *Anat. Rec.* **198**, 183–192 (1980).
- A. V. Graça-Souza, C. Maya-Monteiro, G. O. Paiva-Silva, G. R. C. Braz, M. C. Paes, M. H. F. Sorgine, M. F. Oliveira, P. L. Oliveira, Adaptations against heme toxicity in blood-feeding arthropods. *Insect Biochem. Mol. Biol.* **36**, 322–335 (2006).
- M. U. Muckenthaler, S. Rivella, M. W. Hentze, B. Galy, A red carpet for iron metabolism. *Cell* **168**, 344–361 (2017).
- M. B. Freitas, J. F. Queiroz, C. I. Dias Gomes, C. B. Collares-Buzato, H. C. Barbosa, A. C. Boschero, C. A. Gonçalves, E. C. Pinheiro, Reduced insulin secretion and glucose intolerance are involved in the fasting susceptibility of common vampire bats. *Gen. Comp. Endocrinol.* **183**, 1–6 (2013).
- M. B. Freitas, A. F. Welker, S. F. Millan, E. C. Pinheiro, Metabolic responses induced by fasting in the common vampire bat *Desmodus rotundus*. *J. Comp. Physiol. B* **173**, 703–707 (2003).
- M. B. Freitas, C. B. C. Passos, R. B. Vasconcelos, E. C. Pinheiro, Effects of short-term fasting on energy reserves of vampire bats (*Desmodus rotundus*). *Comp. Biochem. Physiol. B Biochem. Mol. Biol.* **140**, 59–62 (2005).
- G. G. Carter, G. S. Wilkinson, Food sharing in vampire bats: Reciprocal help predicts donations more than relatedness or harassment. *Proc. Biol. Sci.* **280**, 20122573 (2013).
- M. L. Zepeda Mendoza, Z. Xiong, M. Escalera-Zamudio, A. K. Runge, J. Thézé, D. Streicker, H. K. Frank, E. Loza-Rubio, S. Liu, O. A. Ryder, J. A. Samaniego Castruita, A. Katzourakis, G. Pacheco, B. Taboada, U. Löber, O. G. Pybus, Y. Li, E. Rojas-Anaya, K. Bohmann, A. Carmona Baez, C. F. Arias, S. Liu, A. D. Greenwood, M. F. Bertelsen, N. E. White, M. Bunce, G. Zhang, T. Sicheritz-Pontén, M. P. T. Gilbert, Hologenomic adaptations underlying the evolution of sanguivory in the common vampire bat. *Nat. Ecol. Evol.* **2**, 659–668 (2018).
- Y. T. Gutiérrez-Guerrero, E. Ibarra-Laclette, C. M. Del Río, J. Barrera-Redondo, E. A. Rebollar, J. Ortega, L. León-Paniagua, A. Urrutia, E. Aguirre-Planter, L. E. Eguarte, Genomic consequences of dietary diversification and parallel evolution due to nectarivory in leaf-nosed bats. *Gigascience* **9**, gaa059 (2020).
- K. Wang, S. Tian, J. Galindo-González, L. M. Dávalos, Y. Zhang, H. Zhao, Molecular adaptation and convergent evolution of frugivory in Old World and neotropical fruit bats. *Mol. Ecol.* **29**, 4366–4381 (2020).
- W. Hong, H. Zhao, Vampire bats exhibit evolutionary reduction of bitter taste receptor genes common to other bats. *Proc. Biol. Sci.* **281**, 20141079 (2014).
- R. Albalat, C. Canestro, Evolution by gene loss. *Nat. Rev. Genet.* **17**, 379–391 (2016).
- V. Sharma, N. Hecker, J. G. Roscito, L. Foerster, B. E. Langer, M. Hiller, A genomics approach reveals insights into the importance of gene losses for mammalian adaptations. *Nat. Commun.* **9**, 1215 (2018).
- N. Hecker, V. Sharma, M. Hiller, Convergent gene losses illuminate metabolic and physiological changes in herbivores and carnivores. *Proc. Natl. Acad. Sci. U.S.A.* **116**, 3036–3041 (2019).
- M. Huelsmann, N. Hecker, M. S. Springer, J. Gatesy, V. Sharma, M. Hiller, Genes lost during the transition from land to water in cetaceans highlight genomic changes associated with aquatic adaptations. *Sci. Adv.* **5**, eaaw6671 (2019).
- D. Jebb, Z. Huang, M. Pippel, G. M. Hughes, K. Lavrichenko, P. Devanna, S. Winkler, L. S. Jermin, E. C. Skirmuntt, A. Katzourakis, L. Burkitt-Gray, D. A. Ray, K. A. M. Sullivan, J. G. Roscito, B. M. Kirilenko, L. M. Dávalos, A. P. Corthals, M. L. Power, G. Jones, R. D. Ransome, D. K. N. Dechmann, A. G. Locatelli, S. J. Puechmaille, O. Fedrigo, E. D. Jarvis, M. Hiller, S. C. Vernes, E. W. Myers, E. C. Teeling, Six reference-quality genomes reveal evolution of bat adaptations. *Nature* **583**, 578–584 (2020).
- A. Scheben, O. M. Ramos, M. Kramer, S. Goodwin, S. Oppenheim, D. J. Becker, M. C. Schatz, N. B. Simmons, A. Siepel, W. Richard Mc Combie, Long-read sequencing reveals rapid evolution of immunity- and cancer-related genes in bats. *bioRxiv* 2020.2009.290502 [Preprint]. 2021.
- D. J. Strick, L. A. Elferink, Rab15 effector protein: A novel protein for receptor recycling from the endocytic recycling compartment. *Mol. Biol. Cell* **16**, 5699–5709 (2005).
- I. M. Stasiak, D. A. Smith, T. Ganz, G. J. Crawshaw, J. D. Hammermueller, D. Bienzle, B. N. Lillie, Iron storage disease (hemochromatosis) and hepcidin response to iron load in two species of pteropodid fruit bats relative to the common vampire bat. *J. Comp. Physiol. B* **188**, 683–694 (2018).
- J. M. Williams, C. A. Duckworth, M. D. Burkitt, A. J. M. Watson, B. J. Campbell, D. M. Pritchard, Epithelial cell shedding and barrier function: A matter of life and death at the small intestinal villus tip. *Vet. Pathol.* **52**, 445–455 (2015).
- M. Uhlen, P. Oksvold, L. Fagerberg, E. Lundberg, K. Jonasson, M. Forsberg, M. Zwahlen, C. Kampf, K. Wester, S. Hober, H. Werners, L. Björling, F. Ponten, Towards a knowledge-based Human Protein Atlas. *Nat. Biotechnol.* **28**, 1248–1250 (2010).
- L. A. Elferink, D. J. Strick, Functional properties of rab15 effector protein in endocytic recycling. *Methods Enzymol.* **403**, 732–743 (2005).
- E. Chen, F. Yang, H. He, Q. Li, W. Zhang, J. Xing, Z. Zhu, J. Jiang, H. Wang, X. Zhao, R. Liu, L. Lei, J. Dong, Y. Pei, Y. Yang, J. Pan, P. Zhang, S. Liu, L. du, Y. Zeng, J. Yang, Alteration of tumor suppressor BMP5 in sporadic colorectal cancer: A genomic and transcriptomic profiling based study. *Mol. Cancer* **17**, 176 (2018).
- M. J. Brookes, S. Hughes, F. E. Turner, G. Reynolds, N. Sharma, T. Ismail, G. Bex, A. McKie, N. Hotchin, G. J. Anderson, T. Iqbal, C. Tselepis, Modulation of iron transport proteins in human colorectal carcinogenesis. *Gut* **55**, 1449–1460 (2006).
- B. A. Neely, M. G. Janech, M. B. Fenton, N. B. Simmons, A. M. Bland, D. J. Becker, Surveying the vampire bat (*Desmodus rotundus*) serum proteome: A resource for identifying immunological proteins and detecting pathogens. *J. Proteome Res.* **20**, 2547–2559 (2021).
- A. D. Mancini, V. Poutout, The fatty acid receptor FFA1/GPR40 a decade later: How much do we know? *Trends Endocrinol. Metab.* **24**, 398–407 (2013).
- M. G. Latour, T. Alquier, E. Oseid, C. Tremblay, T. L. Jetton, J. Luo, D. C. H. Lin, V. Poutout, GPR40 is necessary but not sufficient for fatty acid stimulation of insulin secretion in vivo. *Diabetes* **56**, 1087–1094 (2007).
- M. G. Pedersen, A. Tagliavini, J. C. Henquin, Calcium signaling and secretory granule pool dynamics underlie biphasic insulin secretion and its amplification by glucose: Experiments and modeling. *Am. J. Physiol. Endocrinol. Metab.* **316**, E475–E486 (2019).
- H. Lan, L. M. Hoos, L. Liu, G. Tetzloff, W. Hu, S. J. Abbondanzo, G. Vassileva, E. L. Gustafson, J. A. Hedrick, H. R. Davis, Lack of FFAR1/GPR40 does not protect mice from high-fat diet-induced metabolic disease. *Diabetes* **57**, 2999–3006 (2008).
- T. Tomita, H. Masuzaki, H. Iwakura, J. Fujikura, M. Noguchi, T. Tanaka, K. Ebihara, J. Kawamura, I. Komoto, Y. Kawaguchi, K. Fujimoto, R. Doi, Y. Shimada, K. Hosoda, M. Imamura, K. Nakao, Expression of the gene for a membrane-bound fatty acid receptor in the pancreas and islet cell tumours in humans: Evidence for GPR40 expression in pancreatic beta cells and implications for insulin secretion. *Diabetologia* **49**, 962–968 (2006).
- S. Del Guerra, M. Bugliani, V. D'Aleo, S. Del Prato, U. Boggi, F. Mosca, F. Filippini, R. Lupi, G-protein-coupled receptor 40 (GPR40) expression and its regulation in human pancreatic islets: The role of type 2 diabetes and fatty acids. *Nutr. Metab. Cardiovasc. Dis.* **20**, 22–25 (2010).
- S. Edfalk, P. Steneberg, H. Edlund, Gpr40 is expressed in enteroendocrine cells and mediates free fatty acid stimulation of incretin secretion. *Diabetes* **57**, 2280–2287 (2008).
- T. Yamashima, Dual effects of the non-esterified fatty acid receptor 'GPR40' for human health. *Prog. Lipid Res.* **58**, 40–50 (2015).
- T. J. Nicolson, E. A. Bellomo, N. Wijesekara, M. K. Loder, J. M. Baldwin, A. V. Gyulkhandanyan, V. Koshkin, A. I. Tarasov, R. Carzaniga, K. Kronenberger, T. K. Taneja, G. da Silva Xavier, S. Libert, P. Froguel, R. Scharfmann, V. Stetsyuk, P. Ravassard, H. Parker, F. M. Gribble, F. Reimann, R. Sladek, S. J. Hughes, P. R. V. Johnson, M. Masseboeuf, R. Burcelin, S. A. Baldwin, M. Liu, R. Lara-Lemus, P. Arvan, F. C. Schuit, M. B. Wheeler, F. Chimienti, G. A. Rutter, Insulin storage and glucose homeostasis in mice null for the granule zinc transporter ZnT8 and studies of the type 2 diabetes-associated variants. *Diabetes* **58**, 2070–2083 (2009).

44. L. D. Pound, S. A. Sarkar, A. Ustione, P. K. Dadi, M. K. Shadoan, C. E. Lee, J. A. Walters, M. Shiota, O. P. McGuinness, D. A. Jacobson, D. W. Piston, J. C. Hutton, D. R. Powell, R. M. O'Brien, The physiological effects of deleting the mouse SLC30A8 gene encoding zinc transporter-8 are influenced by gender and genetic background. *PLOS ONE* **7**, e40972 (2012).
45. F. Chimenti, S. Devergnas, A. Favier, M. Seve, Identification and cloning of a beta-cell-specific zinc transporter, Znt-8, localized into insulin secretory granules. *Diabetes* **53**, 2330–2337 (2004).
46. M. F. Dunn, Zinc-ligand interactions modulate assembly and stability of the insulin hexamer – a review. *Biomaterials* **18**, 295–303 (2005).
47. M. Burguera, J. L. Burguera, O. M. Alarcón, Flow injection and microwave-oven sample decomposition for determination of copper, zinc and iron in whole blood by atomic absorption spectrometry. *Anal. Chim. Acta* **179**, 351–357 (1986).
48. J. M. Peres, S. Bouhallab, C. Petit, F. Bureau, J. L. Maubois, P. Arhan, D. Bouglé, Improvement of zinc intestinal absorption and reduction of zinc/iron interaction using metal bound to the caseinophosphopeptide 1-25 of β -casein. *Reprod. Nutr. Dev.* **38**, 465–472 (1998).
49. P. Kondaiah, P. A. Sharp, R. Pullakhandam, Zinc induces iron egress from intestinal Caco-2 cells via induction of Hephaestin: A role for P13K in intestinal iron absorption. *Biochem. Biophys. Res. Commun.* **523**, 987–992 (2020).
50. L. D. Pound, S. A. Sarkar, R. K. P. Benninger, Y. Wang, A. Suwanichkul, M. K. Shadoan, R. L. Printz, J. K. Oeser, C. E. Lee, D. W. Piston, O. P. McGuinness, J. C. Hutton, D. R. Powell, R. M. O'Brien, Deletion of the mouse SLC30A8 gene encoding zinc transporter-8 results in impaired insulin secretion. *Biochem. J.* **421**, 371–376 (2009).
51. K. J. Bosma, K. E. Syring, J. K. Oeser, J. D. Lee, R. K. P. Benninger, M. E. Pamerter, R. M. O'Brien, Evidence that evolution of the diabetes susceptibility gene SLC30A8 that encodes the zinc transporter Znt8 drives variations in pancreatic islet zinc content in multiple species. *J. Mol. Evol.* **87**, 147–151 (2019).
52. P. D. Zalewski, S. H. Millard, I. J. Forbes, O. Kapaniris, A. Slavotinek, W. H. Betts, A. D. Ward, S. F. Lincoln, I. Mahadevan, Video image analysis of labile zinc in viable pancreatic islet cells using a specific fluorescent probe for zinc. *J. Histochem. Cytochem.* **42**, 877–884 (1994).
53. J. R. Hunt, Bioavailability of iron, zinc, and other trace minerals from vegetarian diets. *Am. J. Clin. Nutr.* **78**, 633S–639S (2003).
54. C. E. Semrad, Zinc and intestinal function. *Curr. Gastroenterol. Rep.* **1**, 398–403 (1999).
55. S. Munro, H. Ceulemans, M. Bollen, J. Duplexico, P. T. W. Cohen, A novel glycogen-targeting subunit of protein phosphatase 1 that is regulated by insulin and shows differential tissue distribution in humans and rodents. *FEBS J.* **272**, 1478–1489 (2005).
56. P. J. Roach, Glycogen and its metabolism. *Curr. Mol. Med.* **2**, 101–120 (2002).
57. M. C. Petersen, D. F. Vatner, G. I. Shulman, Regulation of hepatic glucose metabolism in health and disease. *Nat. Rev. Endocrinol.* **13**, 572–587 (2017).
58. W. G. Aschenbach, Y. Suzuki, K. Breeden, C. Prats, M. F. Hirshman, S. D. Dufresne, K. Sakamoto, P. G. Vilaro, M. Steele, J. H. Kim, S. L. Jing, L. J. Goodyear, A. A. DePaoli-Roach, The muscle-specific protein phosphatase PPT1G/RGL(GM) is essential for activation of glycogen synthase by exercise. *J. Biol. Chem.* **276**, 39959–39967 (2001).
59. M. B. Mehta, S. V. Shewale, R. N. Sequeira, J. S. Millar, N. J. Hand, D. J. Rader, Hepatic protein phosphatase 1 regulatory subunit 3B (Ppp1r3b) promotes hepatic glycogen synthesis and thereby regulates fasting energy homeostasis. *J. Biol. Chem.* **292**, 10444–10454 (2017).
60. S. M. Crosson, A. Khan, J. Printen, J. E. Pessin, A. R. Saltiel, PTG gene deletion causes impaired glycogen synthesis and developmental insulin resistance. *J. Clin. Invest.* **111**, 1423–1432 (2003).
61. Y. Zhang, J. Gu, L. Wang, Z. Zhao, Y. Pan, Y. Chen, Ablation of PPP1R3G reduces glycogen deposition and mitigates high-fat diet induced obesity. *Mol. Cell. Endocrinol.* **439**, 133–140 (2017).
62. N. Zaidi, C. Hermann, T. Herrmann, H. Kalbacher, Emerging functional roles of cathepsin E. *Biochem. Biophys. Res. Commun.* **377**, 327–330 (2008).
63. T. Saku, H. Sakai, Y. Shibata, Y. Kato, K. Yamamoto, An immunocytochemical study on distinct intracellular localization of cathepsin E and cathepsin D in human gastric cells and various rat cells. *J. Biochem.* **110**, 956–964 (1991).
64. G. R. Ordoñez, L. W. Hillier, W. C. Warren, F. Grützner, C. López-Otin, X. S. Puente, Loss of genes implicated in gastric function during platypus evolution. *Genome Biol.* **9**, R81 (2008).
65. V. Sharma, M. Hiller, Losses of human disease-associated genes in placental mammals. *NAR Genom. Bioinform.* **2**, lqz012 (2020).
66. A. Bertolotti, X. Z. Wang, I. Novoa, R. Jungreis, K. Schlessinger, J. H. Cho, A. B. West, D. Ron, Increased sensitivity to dextran sodium sulfate colitis in IRE1 β deficient mice. *J. Clin. Invest.* **107**, 585–593 (2001).
67. J. Iqbal, K. Dai, T. Seimon, R. Jungreis, M. Oyadomari, G. Kuriakose, D. Ron, I. Tabas, M. M. Hussain, IRE1 β inhibits chylomicron production by selectively degrading MTP mRNA. *Cell Metab.* **7**, 445–455 (2008).
68. J. Iqbal, J. Queiroz, Y. Li, X. C. Jiang, D. Ron, M. M. Hussain, Increased intestinal lipid absorption caused by IRE1 β deficiency contributes to hyperlipidemia and atherosclerosis in apolipoprotein E-deficient mice. *Circ. Res.* **110**, 1575–1584 (2012).
69. D. C. Whitcomb, M. E. Lowe, Human pancreatic digestive enzymes. *Dig. Dis. Sci.* **52**, 1–17 (2007).
70. D. Sun, H. Jin, J. Zhang, X. Tan, Integrated whole genome microarray analysis and immunohistochemical assay identifies COL11A1, GJB2 and CTRL as predictive biomarkers for pancreatic cancer. *Cancer Cell Int.* **18**, 174 (2018).
71. D. Mosztbacher, Z. Jancso, M. Sahin-Toth, Loss of chymotrypsin-like protease (CTRL) alters intrapancreatic protease activation but not pancreatitis severity in mice. *Sci. Rep.* **10**, 11731 (2020).
72. T. L. Hostelley, J. E. Nesmith, E. Larkin, A. Jones, D. Boyes, C. C. Leitch, M. Fontaine, N. A. Zaghoul, Exocrine pancreas proteases regulate β -cell proliferation in zebrafish ciliopathy models and in murine systems. *Biol. Open* **10**, (2021).
73. G. G. Carter, G. S. Wilkinson, Common vampire bat contact calls attract past food-sharing partners. *Anim. Behav.* **116**, 45–51 (2016).
74. I. Razik, B. K. G. Brown, R. A. Page, G. G. Carter, Non-kin adoption in the common vampire bat. *R. Soc. Open Sci.* **8**, 201927 (2021).
75. J. Li-Hawkins, E. G. Lund, A. D. Bronson, D. W. Russell, Expression cloning of an oxysterol α -hydroxylase selective for 24-hydroxycholesterol. *J. Biol. Chem.* **275**, 16543–16549 (2000).
76. I. P. Grabovec, S. V. Smolskaya, A. V. Baranovsky, V. N. Zhabinskii, Y. V. Dichenko, P. S. Shabunya, S. A. Usanov, N. V. Strushkevich, Ligand-binding properties and catalytic activity of the purified human 24-hydroxycholesterol 7 α -hydroxylase, CYP39A1. *J. Steroid Biochem. Mol. Biol.* **193**, 105416 (2019).
77. M. Norlin, A. Toll, I. Björkhem, K. Wikvall, 24-hydroxycholesterol is a substrate for hepatic cholesterol 7 α -hydroxylase (CYP7A). *J. Lipid Res.* **41**, 1629–1639 (2000).
78. A. V. Yantsevich, Y. V. Dichenko, F. MacKenzie, D. V. Mukha, A. V. Baranovsky, A. A. Gilep, S. A. Usanov, N. V. Strushkevich, Human steroid and oxysterol 7 α -hydroxylase CYP7B1: Substrate specificity,azole binding and misfolding of clinically relevant mutants. *FEBS J.* **281**, 1700–1713 (2014).
79. C. Knabe, T. Sudhop, K. von Bergmann, D. Lütjohann, Degradation of 24S-hydroxycholesterol in men is not regulated by CYP7A1. *Int. J. Clin. Pharmacol. Ther.* **45**, 577–582 (2007).
80. D. W. Russell, R. W. Halford, D. M. O. Ramirez, R. Shah, T. Kotti, Cholesterol 24-hydroxylase: An enzyme of cholesterol turnover in the brain. *Annu. Rev. Biochem.* **78**, 1017–1040 (2009).
81. D. Lütjohann, O. Breuer, G. Ahlborg, I. Nennesmo, A. Sidén, U. Diczfalusy, I. Björkhem, Cholesterol homeostasis in human brain: Evidence for an age-dependent flux of 24S-hydroxycholesterol from the brain into the circulation. *Proc. Natl. Acad. Sci.* **93**, 9799–9804 (1996).
82. A. R. Stiles, J. Kozlitina, B. M. Thompson, J. G. McDonald, K. S. King, D. W. Russell, Genetic, anatomic, and clinical determinants of human serum sterol and vitamin D levels. *Proc. Natl. Acad. Sci. U.S.A.* **111**, E4006–E4014 (2014).
83. S. M. Paul, J. J. Doherty, A. J. Robichaud, G. M. Belfort, B. Y. Chow, R. S. Hammond, D. C. Crawford, A. J. Linsenbardt, H. J. Shu, Y. Izumi, S. J. Mennerick, C. F. Zorumski, The major brain cholesterol metabolite 24(S)-hydroxycholesterol is a potent allosteric modulator of N-methyl-D-aspartate receptors. *J. Neurosci.* **33**, 17290–17300 (2013).
84. X. Wei, T. Nishi, S. Kondou, H. Kimura, I. Mody, Preferential enhancement of GluN2B-containing native NMDA receptors by the endogenous modulator 24S-hydroxycholesterol in hippocampal neurons. *Neuropharmacology* **148**, 11–20 (2019).
85. S. Maioli, A. Bävner, Z. Ali, M. Heverin, M. A. M. Ismail, E. Puerta, M. Olin, A. Saeed, M. Shafaati, P. Parini, A. Cedazo-Minguez, I. Björkhem, Is it possible to improve memory function by upregulation of the cholesterol 24S-hydroxylase (CYP46A1) in the brain? *PLOS ONE* **8**, e68534 (2013).
86. T. J. Kotti, D. M. O. Ramirez, B. E. Pfeiffer, K. M. Huber, D. W. Russell, Brain cholesterol turnover required for geranylgeraniol production and learning in mice. *Proc. Natl. Acad. Sci. U.S.A.* **103**, 3869–3874 (2006).
87. M. Radosevic, J. Planagumà, F. Mannara, A. Mellado, E. Aguilar, L. Sabater, J. Landa, A. García-Serra, E. Maudes, X. Gasull, M. Lewis, J. Dalmau, Allosteric modulation of NMDARs reverses patients' autoantibody effects in mice. *Neural. Neuroimmunol. Neuroinflamm.* **9**, e1122 (2022).
88. I. Zoicas, J. Kornhuber, The role of the N-methyl-D-aspartate receptors in social behavior in rodents. *Int. J. Mol. Sci.* **20**, (2019).
89. S. P. Ripperger, G. G. Carter, N. Duda, A. Koelbin, B. Cassens, R. Kapitza, D. Josic, J. Berrio-Martinez, R. A. Page, F. Mayer, Vampire bats that cooperate in the lab maintain their social networks in the wild. *Curr. Biol.* **29**, 4139–4144.e4 (2019).
90. G. Baron, H. Stephan, H. D. Frahm, *Comparative Neurobiology in Chiroptera: Brain Characteristics in Functional Systems, Ecoethological Adaptation, Adaptive Radiation, and Evolution* (Springer, 1996).

91. H. Monyer, N. Burnashev, D. J. Laurie, B. Sakmann, P. H. Seeburg, Developmental and regional expression in the rat brain and functional properties of four NMDA receptors. *Neuron* **12**, 529–540 (1994).
92. M. Cardoso-Moreira, J. Halbert, D. Vallotton, B. Velten, C. Chen, Y. Shao, A. Liechti, K. Ascenção, C. Rummel, S. Ovchinnikova, P. V. Mazin, I. Xenarios, K. Harshman, M. Mort, D. N. Cooper, C. Sandi, M. J. Soares, P. G. Ferreira, S. Afonso, M. Carneiro, J. M. A. Turner, J. L. VandeBerg, A. Fallahshahroudi, P. Jensen, R. Behr, S. Lisgo, S. Lindsay, P. Khaitovich, W. Huber, J. Baker, S. Anders, Y. E. Zhang, H. Kaessmann, Gene expression across mammalian organ development. *Nature* **571**, 505–509 (2019).
93. C. C. Wang, R. G. Held, S. C. Chang, L. Yang, E. Delpire, A. Ghosh, B. J. Hall, A critical role for GluN2B-containing NMDA receptors in cortical development and function. *Neuron* **72**, 789–805 (2011).
94. S. Kohl, F. Coppieters, F. Meire, S. Schaich, S. Roosing, C. Brennenstuhl, S. Bolz, M. van Genderen, F. C. Riemsdijk, European Retinal Disease Consortium, R. Lukowski, A. den Hollander, F. P. Cremers, E. de Baere, C. B. Hoyng, B. Wissinger, A nonsense mutation in PDE6H causes autosomal-recessive incomplete achromatopsia. *Am. J. Hum. Genet.* **91**, 527–532 (2012).
95. C. Brennenstuhl, N. Tanimoto, M. Burkard, R. Wagner, S. Bolz, D. Trifunovic, C. Kabagema-Bilan, F. Paquet-Durand, S. C. Beck, G. Huber, M. W. Seeliger, P. Ruth, B. Wissinger, R. Lukowski, Targeted ablation of the Pde6h gene in mice reveals cross-species differences in cone and rod phototransduction protein isoform inventory. *J. Biol. Chem.* **290**, 10242–10255 (2015).
96. B. Chang, T. Grau, S. Dangel, R. Hurd, B. Jurklics, E. C. Sener, S. Andreasson, H. Dollfus, B. Baumann, S. Bolz, N. Artemyev, S. Kohl, J. Heckenlively, B. Wissinger, A homologous genetic basis of the murine cpfl1 mutant and human achromatopsia linked to mutations in the PDE6C gene. *Proc. Natl. Acad. Sci. U.S.A.* **106**, 19581–19586 (2009).
97. T. Grau, N. O. Artemyev, T. Rosenberg, H. Dollfus, O. H. Haugen, E. Cumhur Sener, B. Jurklics, S. Andreasson, C. Kernstock, M. Larsen, E. Zrenner, B. Wissinger, S. Kohl, Decreased catalytic activity and altered activation properties of PDE6C mutants associated with autosomal recessive achromatopsia. *Hum. Mol. Genet.* **20**, 719–730 (2011).
98. C. A. Emerling, A. D. Widjaja, N. N. Nguyen, M. S. Springer, Their loss is our gain: Regressive evolution in vertebrates provides genomic models for uncovering human disease loci. *J. Med. Genet.* **54**, 787–794 (2017).
99. U. Gröger, L. Wiegrebe, Classification of human breathing sounds by the common vampire bat, *Desmodus rotundus*. *BMC Biol* **4**, 18 (2006).
100. M. Escalera-Zamudio, M. L. Zepeda-Mendoza, E. Loza-Rubio, E. Rojas-Anaya, M. L. Méndez-Ojeda, C. F. Arias, A. D. Greenwood, The evolution of bat nucleic acid-sensing Toll-like receptors. *Mol. Ecol.* **24**, 5899–5909 (2015).
101. D. J. Castillo, R. F. Rifkin, D. A. Cowan, M. Potgieter, The healthy human blood microbiome: Fact or fiction? *Front. Cell. Infect. Microbiol.* **9**, 148 (2019).
102. F. Rademacher, S. Dreyer, V. Kopfnagel, R. Gläser, T. Werfel, J. Harder, The antimicrobial and immunomodulatory function of RNase 7 in skin. *Front. Immunol.* **10**, 2553 (2019).
103. T. E. Eichler, B. Becknell, R. S. Easterling, S. E. Ingraham, D. M. Cohen, A. L. Schwaderer, D. S. Hains, B. Li, A. Cohen, J. Metheny, S. Tridandapani, J. D. Spencer, Insulin and the phosphatidylinositol 3-kinase signaling pathway regulate Ribonuclease 7 expression in the human urinary tract. *Kidney Int.* **90**, 568–579 (2016).
104. A. Rodríguez-Carlos, V. Trujillo, I. Gonzalez-Curiel, S. Marin-Luevano, F. Torres-Juarez, A. Santos-Mena, C. Rivas-Santiago, J. A. Enciso-Moreno, V. Zaga-Clavellina, B. Rivas-Santiago, Host defense peptide RNase 7 is down-regulated in the skin of diabetic patients with or without chronic ulcers, and its expression is altered with metformin. *Arch. Med. Res.* **51**, 327–335 (2020).
105. L. M. Bergner, R. J. Orton, A. da Silva Filipe, A. E. Shaw, D. J. Becker, C. Tello, R. Biek, D. G. Streicker, Using noninvasive metagenomics to characterize viral communities from wildlife. *Mol. Ecol. Resour.* **19**, 128–143 (2019).
106. N. Hecker, V. Sharma, M. Hiller, Transition to an aquatic habitat permitted the repeated loss of the pleiotropic KLK8 gene in mammals. *Genome Biol. Evol.* **9**, 3179–3188 (2017).
107. V. Sharma, M. Hiller, Loss of enzymes in the bile acid synthesis pathway explains differences in bile composition among mammals. *Genome Biol. Evol.* **10**, 3211–3217 (2018).
108. N. Mast, A. Saadane, A. Valencia-Olvera, J. Constans, E. Maxfield, H. Arakawa, Y. Li, G. Landreth, I. A. Pikuleva, Cholesterol-metabolizing enzyme cytochrome P450 46A1 as a pharmacologic target for Alzheimer's disease. *Neuropharmacology* **123**, 465–476 (2017).
109. V. Sharma, M. Hiller, Increased alignment sensitivity improves the usage of genome alignments for comparative gene annotation. *Nucleic Acids Res.* **45**, 8369–8377 (2017).
110. V. Sharma, A. Elghafari, M. Hiller, Coding exon-structure aware realigner (CESAR) utilizes genome alignments for accurate comparative gene annotation. *Nucleic Acids Res.* **44**, e103 (2016).
111. H. Cheng, G. T. Concepcion, X. Feng, H. Zhang, H. Li, Haplotype-resolved de novo assembly using phased assembly graphs with hifiasm. *Nat. Methods* **18**, 170–175 (2021).
112. J. Ghurye, A. Rhie, B. P. Walenz, A. Schmitt, S. Selvaraj, M. Pop, A. M. Phillippy, S. Koren, Integrating Hi-C links with assembly graphs for chromosome-scale assembly. *PLoS Comput. Biol.* **15**, e1007273 (2019).
113. H. Li, R. Durbin, Fast and accurate long-read alignment with Burrows-Wheeler transform. *Bioinformatics* **26**, 589–595 (2010).
114. N. Abdennur, L. A. Mirny, Cooler: Scalable storage for Hi-C data and other genomically labeled arrays. *Bioinformatics* **36**, 311–316 (2020).
115. P. Kerpedjiev, N. Abdennur, F. Lekschas, C. McCallum, K. Dinkla, H. Strobelt, J. M. Luber, S. B. Ouellette, A. Azhir, N. Kumar, J. Hwang, S. Lee, B. H. Alver, H. Pfister, L. A. Mirny, P. J. Park, N. Gehlenborg, HiGlass: Web-based visual exploration and analysis of genome interaction maps. *Genome Biol.* **19**, 125 (2018).
116. W. Shen, S. Le, Y. Li, F. Hu, SeqKit: A cross-platform and ultrafast toolkit for FASTA/Q file manipulation. *PLOS ONE* **11**, e0163962 (2016).
117. R. Poplin, P. C. Chang, D. Alexander, S. Schwartz, T. Colthurst, A. Ku, D. Newburger, J. Dijamco, N. Nguyen, P. T. Afshar, S. S. Gross, L. Dorfman, C. Y. McLean, M. A. DePristo, A universal SNP and small-indel variant caller using deep neural networks. *Nat. Biotechnol.* **36**, 983–987 (2018).
118. A. Rhie, B. P. Walenz, S. Koren, A. M. Phillippy, Merqury: Reference-free quality, completeness, and phasing assessment for genome assemblies. *Genome Biol.* **21**, 245 (2020).
119. P. Danecek, J. K. Bonfield, J. Liddle, J. Marshall, V. Ohan, M. O. Pollard, A. Whitwham, T. Keane, S. A. McCarthy, R. M. Davies, H. Li, Twelve years of SAMtools and BCFtools. *Gigascience* **10**, (2021).
120. R. S. Harris, "Improved pairwise alignment of genomic DNA," thesis, The Pennsylvania State University (2007).
121. W. J. Kent, R. Baertsch, A. Hinrichs, W. Miller, D. Haussler, Evolution's cauldron: Duplication, deletion, and rearrangement in the mouse and human genomes. *Proc. Natl. Acad. Sci. U.S.A.* **100**, 11484–11489 (2003).
122. E. Osipova, N. Hecker, M. Hiller, RepeatFiller newly identifies megabases of aligning repetitive sequences and improves annotations of conserved non-exonic elements. *Gigascience* **8**, (2019).
123. H. G. Suarez, B. E. Langer, P. Ladde, M. Hiller, chainCleaner improves genome alignment specificity and sensitivity. *Bioinformatics* **33**, 1596–1603 (2017).
124. V. Sharma, P. Schwede, M. Hiller, CESAR 2.0 substantially improves speed and accuracy of comparative gene annotation. *Bioinformatics* **33**, 3985–3987 (2017).
125. C. M. Lee, G. P. Barber, J. Casper, H. Clawson, M. Diekhans, J. N. Gonzalez, A. S. Hinrichs, B. T. Lee, L. R. Nassar, C. C. Powell, B. J. Raney, K. R. Rosenbloom, D. Schmelzer, M. L. Speir, A. S. Zweig, D. Haussler, M. Haussler, R. M. Kuhn, W. J. Kent, UCSC Genome Browser enters 20th year. *Nucleic Acids Res.* **48**, D756–D761 (2020).
126. V. Ranwez, E. J. P. Douzery, C. Cambon, N. Chantret, F. Delsuc, MACSE v2: Toolkit for the alignment of coding sequences accounting for frameshifts and stop codons. *Mol. Biol. Evol.* **35**, 2582–2584 (2018).
127. A. Di Franco, R. Poujol, D. Baurain, H. Philippe, Evaluating the usefulness of alignment filtering methods to reduce the impact of errors on evolutionary inferences. *BMC Evol. Biol.* **19**, 21 (2019).
128. J. O. Wertheim, B. Murrell, M. D. Smith, S. L. Kosakovsky Pond, K. Scheffler, RELAX: Detecting relaxed selection in a phylogenetic framework. *Mol. Biol. Evol.* **32**, 820–832 (2015).
129. A. Dobin, C. A. Davis, F. Schlesinger, J. Drenkow, C. Zaleski, S. Jha, P. Batut, M. Chaisson, T. R. Gingeras, STAR: Ultrafast universal RNA-seq aligner. *Bioinformatics* **29**, 15–21 (2013).
130. J. T. Robinson, H. Thorvaldsdóttir, W. Winckler, M. Guttman, E. S. Lander, G. Getz, J. P. Mesirov, Integrative genomics viewer. *Nat. Biotechnol.* **29**, 24–26 (2011).
131. P. Virtanen, R. Gommers, T. E. Oliphant, M. Haberland, T. Reddy, D. Cournapeau, E. Burovski, P. Peterson, W. Weckesser, J. Bright, S. J. van der Walt, M. Brett, J. Wilson, K. J. Millman, N. Mayorov, A. R. J. Nelson, E. Jones, R. Kern, E. Larson, C. J. Carey, Í. Polat, Y. Feng, E. W. Moore, J. V. Plas, D. Laxalde, J. Perktold, R. Cimrman, I. Henriksen, E. A. Quintero, C. R. Harris, A. M. Archibald, A. H. Ribeiro, F. Pedregosa, P. van Mulbregt; SciPy 1.0 Contributors, SciPy 1.0: Fundamental algorithms for scientific computing in Python. *Nat. Methods* **17**, 261–272 (2020).
132. C. S. Rouk, B. P. Glass, Comparative gastric histology of five North and Central American bats. *J. Mammal.* **51**, 455–490 (1970).
133. H. Park, E. R. Hall, The gross anatomy of the tongues and stomachs of eight new world bats. *Trans. Kans. Acad. Sci.* **54**, 64–72 (1951).
134. W. A. Wimsatt, A. Gueriere, Observations on the feeding capacities and excretory functions of captive vampire Bats. *J. Mammal.* **43**, 17–27 (1962).
135. D. W. Russell, The enzymes, regulation, and genetics of bile acid synthesis. *Annu. Rev. Biochem.* **72**, 137–174 (2003).
136. E. G. Lund, C. Xie, T. Kotti, S. D. Turley, J. M. Dietschy, D. W. Russell, Knockout of the cholesterol 24-hydroxylase gene in mice reveals a brain-specific mechanism of cholesterol turnover. *J. Biol. Chem.* **278**, 22980–22988 (2003).

137. L. Li, H. Chi, H. Liu, Y. Xia, D. M. Irwin, S. Zhang, Y. Liu, Retention and losses of ultraviolet-sensitive visual pigments in bats. *Sci. Rep.* **8**, 11933 (2018).
138. K. Kries, M. A. S. Barros, G. Duytschaever, J. D. Orkin, M. C. Janiak, D. M. A. Pessoa, A. D. Melin, Colour vision variation in leaf-nosed bats (Phyllostomidae): Links to cave roosting and dietary specialization. *Mol. Ecol.* **27**, 3627–3640 (2018).
139. A. Sadier, K. T. J. Davies, L. R. Yohe, K. Yun, P. Donat, B. P. Hedrick, E. R. Dumont, L. M. Dávalos, S. J. Rossiter, K. E. Sears, Multifactorial processes underlie parallel opsin loss in neotropical bats. *eLife* **7**, (2018).
140. B. F. Simoes, N. M. Foley, G. M. Hughes, H. Zhao, S. Zhang, S. J. Rossiter, E. C. Teeling, As blind as a bat? Opsin phylogenetics illuminates the evolution of color vision in bats. *Mol. Biol. Evol.* **36**, 54–68 (2019).

Acknowledgments: We would like to thank the UCSC genome browser group for providing software and genome annotations and the Computer Service Facilities of the MPI-CBG and MPI-PKS for support. We also thank the Genome Technology Center (RGTC) at Radboudumc for the use of the Sequencing Core Facility (Nijmegen, The Netherlands). Furthermore, we want to thank R. Cornman for support concerning the *Aeorestes cinereus* assembly, D. Lagman and D. Larhammar for helpful feedback on the phototransduction cascade, and V. Mendoza Sáenz and J. Flanders for providing photographs of *D. rotundus* before and after feeding. Figure 3C and figs. S4 and S3A were created with BioRender (<https://biorender.com>).

Funding: This work was supported by the Max Planck Society, the National Council for Scientific and Technological Development (CNPq, Brazil), funding from Environmental

Services & Support (ESS) for fieldwork in Suriname, and the LOEWE Center for Translational Biodiversity Genomics (TBG) funded by the Hessen State Ministry of Higher Education, Research, and the Arts (HMWK). **Author contributions:** M.B. performed the gene loss analysis and analyzed all data. M.F. and B.K.L. provided tissues for genome sequencing. C.G. sequenced the genome. T.B., M.P., and T.S. assembled the genome. A.E.M., D.J., N.H., A.-W.A., and B.M.K. contributed to the genome analysis. M.B.F., A.L.D., and J.A.O. sampled bats and performed iron level measurements. A.J. cosupervised the study. M.H. conceived and supervised the study. M.B. and M.H. made figures and wrote the manuscript with input from all authors. All authors approved the final manuscript. **Competing interests:** The authors declare that they have no competing interests. **Data and materials availability:** All data needed to evaluate the conclusions in the paper are present in the paper and/or the Supplementary Materials. In particular, iron concentrations determined with atomic absorption spectrophotometry are provided in table S5, and tables S1, S2, and S4 list accession numbers of publicly available data that were used in this study. The haplotype-resolved *D. rotundus* assembly and the TOGA annotations are available at <https://bds.mpi-cbg.de/hillerlab/VampireBatGenome/>. The sequencing data and genome assembly are also available at NCBI (BioProject ID PRJNA789159 and BioSample ID SAMN24060601).

Submitted 1 October 2021

Accepted 3 February 2022

Published 25 March 2022

10.1126/sciadv.abm6494

Gene losses in the common vampire bat illuminate molecular adaptations to blood feeding

Moritz Blumer, Tom Brown, Mariella Bontempo Freitas, Ana Luiza Destro, Juraci A. Oliveira, Ariadna E. Morales, Tilman Schell, Carola Greve, Martin Pippel, David Jebb, Nikolai Hecker, Alexis-Walid Ahmed, Bogdan M. Kirilenko, Maddy Foote, Axel Janke, Burton K. Lim, and Michael Hiller

Sci. Adv., **8** (12), eabm6494.
DOI: 10.1126/sciadv.abm6494

View the article online

<https://www.science.org/doi/10.1126/sciadv.abm6494>

Permissions

<https://www.science.org/help/reprints-and-permissions>

Use of this article is subject to the [Terms of service](#)

Science Advances (ISSN) is published by the American Association for the Advancement of Science. 1200 New York Avenue NW, Washington, DC 20005. The title *Science Advances* is a registered trademark of AAAS.
Copyright © 2022 The Authors, some rights reserved; exclusive licensee American Association for the Advancement of Science. No claim to original U.S. Government Works. Distributed under a Creative Commons Attribution NonCommercial License 4.0 (CC BY-NC).